Complex hygroscopic behaviour of ambient aerosol particles revealed by a piezoelectric technique

Christi Jose[1], Aishwarya Singh[1], Kavyashree N Kalkura[1], George V Jose[2], Shailina Srivastava[1], Rameshchan K A[3], Shweta Yadav[4], R. Ravikrishna[1], Meinrat O. Andreae[5], Scot T. Martin[6], Pengfei Liu[7], and Sachin S Gunthe[8]

[1]Indian Institute of Technology Madras
[2]Indian Institute of Technology Bombay
[3]College of Engineering Munnar
[4]Central University of Jammu
[5]Max Planck Institute for Chemistry
[6]Harvard University
[7]Georgia Institute of Technology
[8]Environmental and Water Resources Engineering Division, Department of Civil Engineering, Indian Institute of Technology Madras, Chennai 600036, India.

November 22, 2023

Abstract

Comprehending the intricate interplay between atmospheric aerosols and water vapour in subsaturated regions is vital for accurate modelling of aerosol–cloud–radiation–climate dynamics. But the microphysical mechanisms governing these interactions with ambient aerosols remain inadequately understood. Here we report results from high-altitude, relatively pristine site in Western-Ghats of India during monsoon, serving as a baseline for climate processes in one of the world's most polluted regions. Utilizing a novel quartz crystal microbalance (QCM) approach, we conducted size-resolved sampling to analyse humidity-dependent growth factors, hygroscopicity, deliquescence behaviour, and aerosol liquid water content (ALWC). Fine-mode aerosols ([?]2.5 μm) exhibited size-dependent interactions with water vapour, contributing significantly to ALWC. Deliquescence was observed in larger aerosols (>180 nm), influenced by organic species, with deliquescence relative humidity (DRH) lower than that of pure inorganic salts. This research highlights the significance of understanding ambient aerosol-water interactions and hygroscopicity for refining climate models in subsaturated conditions.

Complex hygroscopic behaviour of ambient aerosol particles revealed by a piezoelectric technique

Christi Jose[1,2], Aishwarya Singh[1,2], Kavyashree N. Kalkura[1,2], George V. Jose[3], Shailina Srivastava[1,2], Rameshchand K. A.[4], Shweta Yadav[5], R. Ravikrishna[2,6], M. O. Andreae[7,8,9], Scot T. Martin[10,11], Pengfei Liu[12,*], and Sachin S. Gunthe[1,2,*]

[1]Environemntal Engineering Division, Dept of Civil Engineering, Indian Institute of Technology Madras, Chennai 600036, India

[2]Centre for Atmospheric and Climate Sciences, Indian Institute of Technology Madras, Chennai 600036, India

[3]Dept of Civil Engineering, Indian Institute of Technology Bombay, Mumbai 400076, India

[4]Dept of Mechanical Engineering, College of Engineering Munnar, Munnar 685612, India

[5]Dept of Environmental Sciences, Central University of Jammu, Samba, Jammu and Kashmir 181143, India

[6]Dept of Chemical Engineering, Indian Institute of Technology Madras, Chennai 600036, India

[7]Multiphase Chemistry Department, Max Planck Institute for Chemistry, 55128 Mainz, Germany

[8]Scripps Institution of Oceanography, University of California San Diego, La Jolla, CA 92093, USA

[9]Department of Geology and Geophysics, King Saud University, Riyadh 11451, Saudi Arabia

[10]Department of Earth and Planetary Sciences, Harvard University, Cambridge, MA 02138, USA

[11]John A. Paulson School of Engineering & Applied Sciences, Harvard University, Cambridge, MA 02138, USA

[12]School of Earth and Atmospheric Sciences, Georgia Institute of Technology, Atlanta, GA 30332, USA

*Correspondence to: Sachin S. Gunthe (s.gunthe@iitm.ac.in) and Pengfei Liu (pengfei.liu@eas.gatech.edu)

KEYPOINTS

- QCM technique revealed aerosol properties at low RH values offering insights that may not be captured by traditional size-based measurements
- The size-dependent variations in aerosol properties below DRH emphasize the need to understand how aerosol properties change with RH history
- Organic in aerosols complicate its cloud forming ability, necessitating additional studies in diverse environments to improve climate models

ABSTRACT

Comprehending the intricate interplay between atmospheric aerosols and water vapour in subsaturated regions is vital for accurate modelling of aerosol–cloud–radiation–climate dynamics. But the microphysical mechanisms governing these interactions with ambient aerosols remain inadequately understood. Here we report results from high-altitude, relatively pristine site in Western-Ghats of India during monsoon, serving as a baseline for climate processes in one of the world's most polluted regions. Utilizing a novel quartz crystal microbalance (QCM) approach, we conducted size-resolved sampling to analyse humidity-dependent growth factors, hygroscopicity, deliquescence behaviour, and aerosol liquid water content (ALWC). Fine-mode aerosols (≤2.5 μm) exhibited size-dependent interactions with water vapour, contributing significantly to ALWC. Deliquescence was observed in larger aerosols (>180 nm), influenced by organic species, with deliquescence relative humidity (DRH) lower than that of pure inorganic salts. This research highlights the significance of understanding ambient aerosol-water interactions and hygroscopicity for refining climate models in subsaturated conditions.

PLAIN LANGUAGE SUMMARY

Aerosol particles interact with water vapour in the atmosphere. Understanding these interactions in sub – and super-saturated regions is crucial because they affect processes such as cloud formation, radiation, and climate. We collected ambient aerosol samples from Western Ghats in India to understand natural processes that happen without significant human interventions. Using a special technique involving a quartz crystal sensor, we measured different aspects, such as how aerosols grow with humidity, their ability to uptake the water molecules, and when they transition from solid to liquid (deliquescence). Interestingly, fine particles, especially those smaller than 2.5 μm, exhibited unique behaviours. While larger particles underwent a transition from solid to liquid under certain conditions, this didn't happen for the smaller particles. These findings highlight the importance of understanding these interactions for more accurate climate predictions.

1. INTRODUCTION

Understanding the hygroscopicity of atmospheric aerosols is crucial for assessing cloud formation and their climate and air pollution impact (Cheung et al., 2015). Investigation of the hygroscopicity of ambient aerosols poses significant challenges due to their chemical complexity, particle size variation, phase state, and viscosity. Techniques like Fourier transform infrared spectroscopy (FTIR) (Y. Liu et al., 2008; Y. Liu & Laskin, 2009), quartz crystal microbalance (QCM) (Chao et al., 2020; Demou et al., 2003; P. Liu et al., 2016a; P. Liu, Song, et al., 2018a), Raman spectroscopy (Ling & Chan, 2008; Y. J. Liu et al., 2008), electrodynamic balance (EDB) (Choi & Chan, 2002; Peng & Chan, 2001; Pope et al., 2010), optical microscopy (OM) (Ahn et al., 2010; Eom et al., 2014; Gupta et al., 2015), hygroscopicity tandem differential mobility analysis (HTDMA) (Cheung et al., 2015; Prenni et al., 2007; Zieger et al., 2017a) and size-selected cloud condensation nuclei (CCN) spectrometry (Petters et al., 2007; Pöhlker et al., 2016; Rose et al., 2008) have been employed to study the hygroscopicity of laboratory – generated and ambient aerosols (Tang et al., 2019). However, a consensus on the most effective method is lacking, leading to inconsistent and incomparable results. Hygroscopicity measurements primarily focus on accumulation mode particles, limiting data on nucleation and coarse mode particles with complex behaviours. Discrepancies in hygroscopic properties and organic and inorganic species composition in atmospheric aerosols result in diverse growth factors and phase transitions, crucial for accurate climate modelling (Li et al., 2021).

The QCM is effective in determining mass–based hygroscopicity and physical property variations of atmospherically–relevant aerosols (Demou et al., 2003; P. Liu et al., 2016b; P. Liu, Song, et al., 2018b). It overcomes the limitations of traditional methods like HTDMA, which has a narrow particle size range with limited relative humidity (RH) resolution (Zhao et al., 2022). Conventional HTDMA methods inadequately reveal hygroscopicity heterogeneity and phase transitions in wider aerosol size range, impacting processes like CCN activation and aerosol liquid water (Li et al., 2021). QCM's mass-based measurements accurately quantify aerosol hygroscopicity behaviour across a wide RH range in the atmosphere, detailing physical property variations during phase transitions and help to delineate water uptake mechanisms, including solubility and water diffusion limitations (P. Liu, Li, et al., 2018; P. Liu, Song, et al., 2018b).

India's climate is distinct and intricate, and as per the 2020 climate change assessment report, India has faced challenges like temperature rise and extreme weather events since the mid-20th century. A key hurdle in addressing these issues is the absence of systematic aerosol characteristic measurements, particularly in aerosol-water vapor interactions in the subsaturated regime (Cheung et al., 2015). Aerosol particles from a forest-surrounded by pristine area are anticipated to contain substantial biogenic organic aerosols. The dynamic chemical transformation of secondary organic aerosols (SOA) in the atmosphere leads to intricate compositions. Atmospheric processing further complicates the understanding of phase state and properties of atmospheric aerosols (Rastak et al., 2017). In this study, QCM measurements are utilized to explore aerosol hygroscopicity dependence on RH, chemical composition, and size across a broad range of ambient aerosols in India's relatively pristine setting.

2. MATERIALS AND METHODS

Size-resolved ambient aerosols were sampled at the Natural Aerosol and Bioaerosol High Altitude (NABHA) Laboratory at the College of Engineering, Munnar (10.0930° N, 77.0682° E; 1600 m above mean sea level), a high-altitude and typically clean site situated in the Western Ghats of India, using a 10-stage micro-orifice uniform deposit impactor (MOUDI-II 120-R, TSI) (V. Marple et al., 2014; V. A. Marple et al., 1991) during the monsoon season (August-September) of 2021. Ambient particles collected on PTFE (Polytetrafluoroethylene) filters were transferred to a hydrophobic SiO_2-coated quartz sensor by gently pressing the filter paper onto the sensor. The hygroscopic growth factor, hygroscopicity parameter and deliquescence relative humidity (DRH) were estimated using a highly sensitive mass balance instrument, QCM (QSense Analyzer, Biolin Scientific) (P. Liu, Song, et al., 2018a; Reviakine et al., 2011). The accuracy and robustness of the method were demonstrated by performing measurements of the hygroscopic growth factor and DRH for sucrose and $(NH_4)_2SO_4$ particles, respectively, which were compared with previously reported results (Arenas et al., 2012a; Chao et al., 2020; Martin, 2000; Norrish, 1966; Peng et al., 2022; Starzak & Peacock, 1997; Zobrist et al., 2011) (Fig. S3 and S4). The hygroscopic growth factor and the corresponding hygroscopicity parameter, κ, were determined over a wide range of RH conditions using κ-Köhler theory (Petters & Kreidenweis, 2007), where κ represents a quantitative measure of aerosol water uptake characteristics and CCN activity (Zhao et al., 2022). The water uptake characteristics and the phase transition behaviours of the ambient

samples were investigated and compared between different size ranges of particles below 10 µm collected using the MOUDI sampler. The Aerosol Liquid Water Content (ALWC) (Bian et al., 2014) at different RH conditions was also estimated from corresponding hygroscopicity parameters for each size range of particles (Fig. S5). The number size distributions of the ambient aerosol particles of size 10 to 420 nm [measured in parallel using a scanning mobility particle sizer – SMPS, comprised of an electrostatic classifier (EC, TSI Model 3082) equipped with a differential mobility analyser (DMA, TSI Model 3081) and a condensation particle counter (CPC, TSI Model 3750)], were then converted to mass size distributions assuming a particle density of 1.2 g cm^{-3} (DeCarlo et al., 2004). The supermicron particle mass size distribution for the same season, but a different year, was used in this study, which had been obtained using an Ultraviolet Aerodynamic Particle Sizer (UV-APS, TSI Inc., model 3314) (Valsan et al., 2016).

Meteorological parameters were recorded using an automatic weather station (AWS, Clima Sensor US) during the sampling period. Figure 1 shows the sampling site – Munnar, along with aerosol optical depth (AOD) over India during the monsoon season, indicating the relatively pristine nature of the sampling site. During the measurement, airmasses predominantly arrived from the southwest direction, bringing clean marine influx to the observational site and resulting in a low influence of anthropogenic emissions (Fig. 1). A more detailed description of the instruments, experimental techniques, and estimation of various parameters is provided in the Supporting Information (SI).

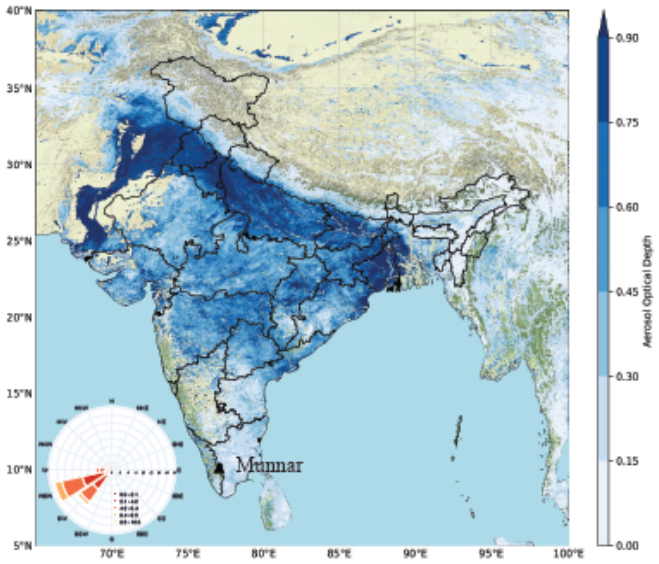

Figure 1. Spatial distribution of average Aerosol Optical Depth (AOD) derived from MODIS (Moderate Resolution Imaging Spectroradiometer) Level 2 data over the Indian continental region during the monsoon season of 2021 (June - September). The AOD distribution clearly indicates a relatively low aerosol loading over the observational site of Munnar (marked as a black triangle) compared with the other parts of India. The wind rose diagram shown in the inset shows the average wind speed and wind direction arriving at the sampling site during the ambient aerosol sampling period (August – September 2021). The prevailing air masses mostly originated over the Indian Ocean and arrived from southwest direction, bringing clean marine influx to the observational site, confirming the relatively low influence of anthropogenic activities.

3. RESULTS AND DISCUSSION

The QCM sensor's oscillation frequency variation (Δf) signifies water uptake and release, providing insights into adsorption, desorption, and physical states of particles during solid-to-aqueous phase transition (Arenas et al., 2012b). Normalizing the frequency shift at higher RH to that of deposited dry sample (RH <5%) yields the percentage value, Δf_N (Chao et al., 2020). Figure 2 shows Δf_N for the ambient aerosol particles across various RH levels and sampled size ranges. A negative sign in Δf_N indicates frequency reduction with increasing RH due to water uptake. Further details of Δf_N and its derivative, $d(\Delta f_N)/(RH)$, are available in SI.

For the particle size <180 nm (Fig. 2a), Δf_N decreased, implying water uptake, with <56 nm particles exhibiting the lowest value. In Figure 2b and 2c, particles showed increased water uptake at lower RH, evidenced by Δf_N decrease. However, Δf_N suddenly increased at specific RH, indicating a drastic water uptake leading to deliquescence-induced phase transition. Figures 2a-c revealed deliquescence in particles >180 nm at different RH (known as DRH), absent in those <180 nm. Past studies reported no deliquescence for ambient and laboratory-generated atmospherically relevant particles even at high RH, attributing them to organic nature (Arenas et al., 2012a; Brooks et al., 2002; Chao et al., 2020; Peng et al., 2022). We hypothesize that particles <180 nm were likely dominated by freshly formed secondary organic aerosols (SOA) from biogenic volatile organic compound (VOC) oxidation, supported by the densely vegetated/forest region and season. Concurrent quasi-continuous measurements during the same campaign indicated upto ~90% organic fraction in NR-PM_1 (non-refractory particulate matter with an aerodynamic diameter ≤1 μm; Tab. S2) with details discussed in subsequent studies.

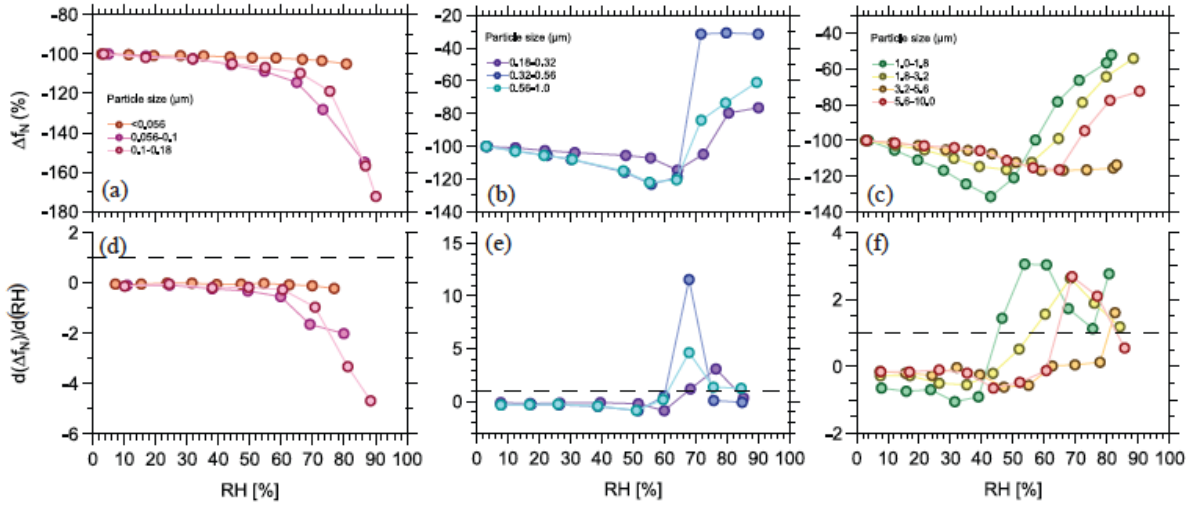

Figure 2. Deliquescence phase transition behaviour of size-resolved ambient aerosol particles from Munnar. For panels a, b, and c, Δf_N represents the change in the oscillation frequency of the quartz crystal microbalance (QCM) sensor resulting due to water uptake by the ambient aerosol particles at different relative humidity (RH) conditions normalized to that of the dry aerosol particles at RH <5%, expressed as percentage. The decrease in the value of Δf_N for each size range for the sampled ambient aerosol particles indicates the water uptake at different RH conditions in the subsaturated regime. The solid markers and lines identify different particle size ranges. In panels d, e, and f, the derivative of Δf_N with respect to RH ($d(\Delta f_N)/d(RH)$) is plotted against RH to determine the deliquescence relative humidity (DRH) value corresponding to the respective aerosol size ranges. The RH values at which $d(\Delta f_N)/d(RH)$ becomes ≥1 (marked by the dotted line) represent the DRH values for the individual aerosol size ranges.

Following Chao et al. (2020), DRH, indicated by $d(\Delta f_N)/(RH) \geq 1$ ranged from ~60 – 68% for three size ranges (180 nm – 320 nm; 320 nm – 560 nm; 560 nm – 1 µm) in this study (Fig. 2e). Above 180 nm, inorganic salts, like $(NH_4)_2SO_4$, may contribute to DRH appearance (Hu et al., 2010) (Fig. 2b,e). These DRH values, smaller than pure $(NH_4)_2SO_4$ (DRH=80%), suggest mixed salts and/or organic compounds in the sampled aerosol particles. The deliquescence behaviour of organic-inorganic mixtures introduces complexity due to solubility limitations, influenced by the organic species in the aerosol particles. Previous studies noted reduced DRH of inorganic species and sometimes, unaffected by organics (Smith et al., 2011, 2012, 2013). Thus, we hypothesize 180 nm to 1 µm particles at this site reflect a complex mixture of inorganic salts like $(NH_4)_2SO_4$ and water-soluble organic compounds. Supermicron particles (>1 µm), except 1 – 1.8 µm, showed <17% Δf_N, indicating lower water uptake (Fig. 2c). Beyond maximum water uptake, the three size ranges exhibited different DRH values. 1.8 – 3.2 µm and 5.6 – 10 µm exhibited DRH between 56 – 68%, suggesting a mixture of water-soluble organic compounds and inorganic salts. However, 3.2 – 5.6 µm showed a very high DRH (>81%) with the organic fraction minimally affecting DRH due to solubility limitations. For 1.8 – 3.2 µm and 5.6 – 10 µm, reduced DRH

compared to pure inorganic salts suggests a mix of water-soluble organic and inorganic compounds (Smith et al., 2011, 2012, 2013). The 1.0 – 1.8 μm range exhibited a >30% Δf_N reduction at ~42% RH, indicating a higher water uptake and the observed DRH appeared to be ~45 – 53%, consistent with the highest κ_m (~0.44, see discussion below) among all measured size ranges (Chao et al., 2020). The low DRH at this site suggests presence of highly water-soluble organic material within the organic-inorganic (sea salt) mixture in this size range.

Figure 3 shows the size-resolved mass-based hygroscopic growth factors (gf_m) and the corresponding mass-based hygroscopicity parameters (κ_m) of ambient aerosol particles calculated from QCM measurements (Text S4 and S5) over a wide RH range (2 – 90%). In Figure 3a, the growth factor increases with water uptake in humid air, showing size-dependent variations across different RH levels (indicated by markers). Each size range had a maximum RH limit beyond which gf_m estimation was impossible due to deliquescence, as observed in previous studies (Chao et al., 2020). Accordingly, the highest gf_m=1.72 was recorded at RH=90% for the 100 – 180 nm particles. The pronounced variations in gf_m between different-sized particles at a given RH indicate varying chemical composition and hygroscopicity across the sampled sizes.

Figure 3b shows the size-dependent average κ_m values, calculated from the gf_m values in Figure 3a. Each particle size range exhibited minimal κ_m variation (average $\kappa_m \pm 0.007$), suggesting ideal solution behaviour across the wide RH range (Z. Wang et al., 2017). The average κ_m values (indicated by dashed lines in Figure 3b) of the size-resolved ambient particles varied significantly between 0.016 (<0.056 nm) and 0.44 (1.0 – 1.8 μm) over the investigated RH range. This implies κ_m as a function of size, and indicates distinct chemical compositions for each size fraction. For example, the small increase in κ_m from 0.016 to 0.078 for particles <56 nm to 56-100 nm, respectively, is potentially owing to aging processes (Zhang et al., 2023). Aerosol particles <320 nm exhibited very low average κ_m (0.06), which may be primarily due to the strong dominance of organic compounds in these size ranges (Demou et al., 2003; Li et al., 2021; Shi et al., 2022). The particles in the size range of 320 nm – 1 μm were moderately hygroscopic (average κ_m=0.19) indicating the influence of inorganic salts (Wu et al., 2016). The particles between 1.0 – 1.8 μm exhibited highest κ_m (0.44), which implies the presence of highly hygroscopic material such as sea salt

(Zieger et al., 2017b) mixed with organic compounds. Even larger particles exhibited reduced κ_m, possibly due to the presence of dust particles (Koehler et al., 2009), transported at this site during monsoon season (Valsan et al., 2016). The κ-Köhler parameterization fit accurately elucidates the gf_m within each size range over a wide range of RH values (Petters & Kreidenweis, 2007).

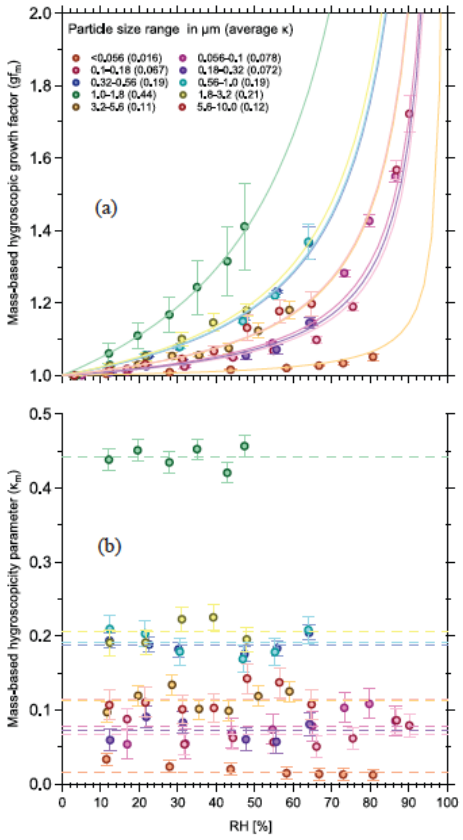

Figure 3. Size-resolved hygroscopicity measurements of ambient aerosol particles at the high-altitude site, Munnar, during the Monsoon season (August-September 2021). (a) Mass-based hygroscopic growth factor (gf_m) derived using a quartz crystal microbalance (QCM) for ten different size ranges of ambient aerosol particles at different relative humidity (RH) conditions in the subsaturated regime (circles). The solid lines represent the corresponding κ-Köhler growth factor fits obtained using the mean value of mass-based hygroscopicity parameters, κ_m. The error bars represent the variations in gf_m averaged over the mass change corresponding to different overtone frequencies of the QCM sensor at respective RH conditions. The values in parentheses are the mean κ_m values corresponding to the respective size ranges. (b) The data points are the κ_m values calculated based on the gf_m (as shown in (a)) using the κ-Köhler theory for different RH conditions in the subsaturated regime. The dotted lines represent the mean κ_m value for each size range of ambient aerosol particles and the error bars represent one standard deviation.

Figure 4 shows the size dependency of κ_m in the subsaturated regime measured by QCM together with κ_{CCN} (Text S2) in the supersaturated regime determined by size-resolved CCN measurements and aerosol size distributions obtained by SMPS and UV-APS. The submicron particles show a bimodal number size distribution with an Aitken mode peak at 63 nm and an accumulation mode at 145 nm, while the mass size distributions peak at 350 nm and 3 µm,

respectively. The average κ_{CCN} increased from a value of 0.28 for the Aitken mode particles to 0.47 for the accumulation mode particles. In the submicron region, κ_m exhibited a nominal increase with particle size (Wu et al., 2016). in parallel with the increase in κ_{CCN}, albeit at much lower absolute values. This increase likely reflects the decrease of organic fraction with size in the submicron range, which is supported by the appearance of deliquescence in the size range above 180 nm, indicating the presence of inorganic salts. In the supermicron region (for particles ≥1 μm), κ_m peaked due to the potential presence of NaCl particles in the size range 1.0 – 1.8 μm, and decreased again in the higher size ranges (>1.8 μm) likely because of the presence of dust particles. The average κ_m value (0.18) obtained from QCM measurements across all the sampled size ranges in the subsaturated regime was lower than the average κ_{CCN} (0.39), likely due to the solubility limitation (Dusek et al., 2011; Hersey et al., 2013; Rastak et al., 2017; Riipinen et al., 2015; Wittbom et al., 2018) of organic and inorganic compounds in ambient aerosol particles below the DRH. Most inorganic species are completely dissolved beyond the DRH point in the subsaturated regime, allowing κ_{CCN} to assume complete particle solubility (Pajunoja et al., 2015; Petters & Kreidenweis, 2007).

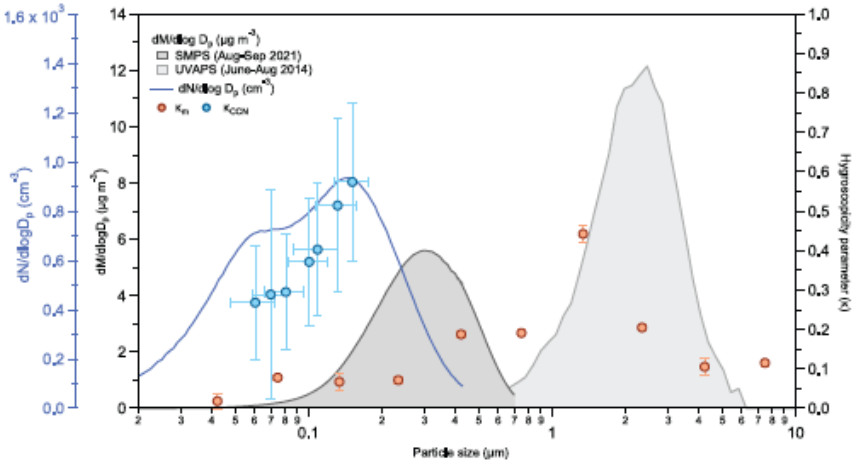

Figure 4. Aerosol size distributions, hygroscopicity parameters derived from quartz crystal microbalance (QCM) experiments (κ_m), and from size-resolved cloud condensation nuclei (CCN) measurements (κ_{CCN}). The number size distribution obtained using a Scanning Mobility Particle Sizer (SMPS) over the size range of 10 – 430 nm (blue curve) was measured during the sampling period and exhibited a bimodal distribution. The mass size distributions (dark grey shaded area) were derived based on the aerosol number size distribution by assuming a density of 1.2 g cm^{-3} for the submicron region. The mass size distribution for the supermicron range (light grey shaded area) was obtained using Ultraviolet Aerodynamic Particle Sizer (UV-APS) measurements during the same season (June-August) but for a different year (2014). The hygroscopicity parameters derived from QCM experiments (κ_m; orange points) and size-resolved CCN measurements (κ_{CCN}; blue points) are shown for the comparison. The error bars for κ_m and κ_{CCN} indicate the measurement uncertainty and variability, respectively.

Unlike QCM measurements, the hygroscopicity parameters obtained in previous studies using the HTDMA technique (κ_{HTDMA}) are often consistent with κ_{CCN}, as the particle

hygroscopicity is determined by particle size increase above DRH point, unaffected by solubility limits (Pajunoja et al., 2015; Y. Wang et al., 2018; Wu et al., 2013). The technical limitations, particularly limited diameter changes corresponding to gf_m values less than 2.0, prevent HTDMA from measuring aerosol hygroscopic properties below the DRH point in the subsaturated regime (Laskina et al., 2015). In contrast, the QCM technique, which is not subject to these limitations, can be used to understand the water uptake characteristics of aerosol particles in the subsaturated regime below DRH and substantially enhance our understanding about solubility limitations of organic and inorganic compounds in the lower RH region. Such an enhancement in the knowledge is crucial for accurately quantifying the radiative forcing effects of ambient aerosol particles in the atmosphere. The strong size dependence of κ_m also indicated varying chemical composition for different size ranges measured in this study.

4. SUMMARY AND ATMOSPHERIC IMPLICATIONS

We report the first results based on a high-sensitivity QCM technique to investigate the mass-based growth factor and hygroscopicity parameter of size–resolved ambient aerosols over a wide range of RH from a relatively pristine high–altitude site in India. For the investigated size ranges, the pronounced variations in gf_m below the DRH provided an opportunity to better understand the changes in ambient aerosol properties even at low RH values, which may not be revealed by size-based growth factor measurements (Hu et al., 2010; Laskina et al., 2015). These measurements clearly highlight the important and critical role in knowing the changes in aerosol properties based on their RH history for an improved understanding of water uptake, phase transition, and radiative impact of atmospheric aerosol particles (Zhao et al., 2022). Based on the estimated κ_m values, the ambient aerosol particles exhibited the behaviour of an ideal solution (Pajunoja et al., 2015) and strong size-dependent chemical composition. We further observed a pronounced size dependency of the DRH values potentially resulting from complexities of organic solubility in organic–inorganic mixtures (Li et al., 2021). Such a complexity owing to the presence of various organic species may alter the CCN behaviour of atmospheric aerosol particles due to phase transitions and changes in physical properties. The understanding of CCN activation in the supersaturated regime under the assumption of complete solubility of particles is relatively well established. But the understanding of the thermodynamic properties associated with particle growth in the subsaturated regime still remains a challenge. Our findings emphasize the need for additional experiments on ambient and atmospherically relevant laboratory-generated aerosol particles

using high-sensitivity techniques like QCM. We demonstrated the importance of this technique to better understand the rapid changes in aerosol properties resulting from exposure to a wide range of atmospheric RH conditions. The enhancement in our understanding of the complex interplay between water vapour and aerosol particles will help in developing more accurate models to effectively describe the role of aerosols in atmospheric processes to reduce climate uncertainties and assess the impact of air pollution on human and ecosystem health.

ASSOCIATED CONTENT

Author contributions

SSG conceived the idea. SSG and PL conceptualized the study and designed the research. CJ further developed and validated the QCM measurements for the ambient aerosol studies. CJ performed the field measurement campaign to collect the aerosol samples with support from AS, KNK, and RKA. CJ performed all the laboratory experiments using QCM with support from SS. GVJ performed the satellite data analysis to obtain the AOD values. CJ carried out the data analysis obtained from QCM with input from PL and SSG. CJ and AS performed the scientific interpretation of the QCM data under the mentorship of RR, SSG and PL. CJ wrote the first draft of manuscript under the mentorship of SSG with inputs from PL and RR, and further edits from SY. MOA and STM further provided critical and valuable inputs on the manuscript.

Open research

The data used in the manuscript has been deposited in an open research repository as Excel files, accessible at https://doi.org/10.6084/m9.figshare.24512377. MODIS data were sourced from the Level 2 and Atmosphere Archive and Distribution System (LAADS) (https://doi.org/10.5067/MODIS/MYD04_3K.061). Figures were prepared using Igor Pro version 9 (WaveMetrics Inc.), licensed by SSG and accessible at https://www.wavemetrics.com/software/igor-pro-9.

Acknowledgments

SSG gratefully acknowledges funding from the Ministry of Earth Sciences (MoES; sanction number MoES/16/20/12-RDEAS dated 31. Mar.2014), Government of India, for the purchase of the Cloud Condensation Nuclei Counter (CCNc). This work was supported by partial funding from the Ministry of Earth Sciences (MoES; sanction number MoES/16/04/2017-APHH (PROMOTE)), the Government of India, and the Department of Science and Technology (sanction number DST/CCP/CoE/141/2018C), the Government of India for the purchase of Quartz Crystal Microbalance (QCM). PL acknowledges the start-up funding support from the Georgia Institute of Technology. CJ acknowledges the Department of Science and Technology, the Government of India for the fellowship. Authors acknowledge the valuable support and help provided by the staff at the College of Engineering Munnar during the campaign, with special and critical help from Jyothish Jose. CJ acknowledges the

428 invaluable assistance provided by Emil Varghese during the laboratory experiments. We are
429 thankful to the support staff from Biolin Scientific, and Specialise Instruments Marketing
430 Company, Mumbai, India for their help during the experiments. We acknowledge the
431 National Aeronautics and Space Administration (NASA) for making Moderate Resolution
432 Imaging Spectroradiometer (MODIS) Earth data available to the user community.

References

Ahn, K. H., Kim, S. M., Jung, H. J., Lee, M. J., Eom, H. J., Maskey, S., & Ro, C. U. (2010). Combined use of optical and electron microscopic techniques for the measurement of hygroscopic property, chemical composition, and morphology of individual aerosol particles. *Analytical Chemistry*, *82*(19), 7999–8009. https://doi.org/10.1021/ac101432y

Arenas, K. J. L., Schill, S. R., Malla, A., & Hudson, P. K. (2012a). Deliquescence phase transition measurements by quartz crystal microbalance frequency shifts. *Journal of Physical Chemistry A*, *116*(29), 7658–7667. https://doi.org/10.1021/jp3016722

Arenas, K. J. L., Schill, S. R., Malla, A., & Hudson, P. K. (2012b). Deliquescence phase transition measurements by quartz crystal microbalance frequency shifts. *Journal of Physical Chemistry A*, *116*(29), 7658–7667. https://doi.org/10.1021/jp3016722

Bian, Y. X., Zhao, C. S., Ma, N., Chen, J., & Xu, W. Y. (2014). A study of aerosol liquid water content based on hygroscopicity measurements at high relative humidity in the North China Plain. *Atmospheric Chemistry and Physics*, *14*(12), 6417–6426. https://doi.org/10.5194/acp-14-6417-2014

Brooks, S. D., Wise, M. E., Cushing, M., & Tolbert, M. A. (2002). Deliquescence behavior of organic/ammonium sulfate aerosol. *Geophysical Research Letters*, *29*(19). https://doi.org/10.1029/2002GL014733

Chao, H. J., Huang, W. C., Chen, C. L., Chou, C. C. K., & Hung, H. M. (2020). Water Adsorption vs Phase Transition of Aerosols Monitored by a Quartz Crystal Microbalance. *ACS Omega*, *5*(49), 31858–31866. https://doi.org/10.1021/acsomega.0c04698

Cheung, H. H. Y., Yeung, M. C., Li, Y. J., Lee, B. P., & Chan, C. K. (2015). Relative Humidity-Dependent HTDMA Measurements of Ambient Aerosols at the HKUST Supersite in Hong Kong, China. *Aerosol Science and Technology*, *49*(8), 643–654. https://doi.org/10.1080/02786826.2015.1058482

Choi, M. Y., & Chan, C. K. (2002). The effects of organic species on the hygroscopic behaviors of inorganic aerosols. *Environmental Science and Technology*, *36*(11), 2422–2428. https://doi.org/10.1021/es0113293

DeCarlo, P. F., Slowik, J. G., Worsnop, D. R., Davidovits, P., & Jimenez, J. L. (2004). Particle morphology and density characterization by combined mobility and aerodynamic diameter measurements. Part 1: Theory. *Aerosol Science and Technology*, *38*(12), 1185–1205. https://doi.org/10.1080/027868290903907

Demou, E., Visram, H., Donaldson, D. J., & Makar, P. A. (2003). Uptake of water by organic films: The dependence on the film oxidation state. *Atmospheric Environment*, *37*(25), 3529–3537. https://doi.org/10.1016/S1352-2310(03)00430-8

Dusek, U., Frank, G. P., Massling, A., Zeromskiene, K., Iinuma, Y., Schmid, O., Helas, G., Hennig, T., Wiedensohler, A., & Andreae, M. O. (2011). Water uptake by biomass burning aerosol at sub-and supersaturated conditions: Closure studies and implications for the role of organics. *Atmospheric Chemistry and Physics*, *11*(18), 9519–9532. https://doi.org/10.5194/acp-11-9519-2011

Eom, H. J., Gupta, D., Li, X., Jung, H. J., Kim, H., & Ro, C. U. (2014). Influence of collecting substrates on the characterization of hygroscopic properties of inorganic aerosol particles. *Analytical Chemistry*, *86*(5), 2648–2656. https://doi.org/10.1021/ac4042075

476 Gupta, D., Kim, H., Park, G., Li, X., Eom, H. J., & Ro, C. U. (2015). Hygroscopic properties of NaCl
477 and NaNO3 mixture particles as reacted inorganic sea-salt aerosol surrogates. *Atmospheric*
478 *Chemistry and Physics*, *15*(6), 3379–3393. https://doi.org/10.5194/acp-15-3379-2015

479 Hersey, S. P., Craven, J. S., Metcalf, A. R., Lin, J., Lathem, T., Suski, K. J., Cahill, J. F., Duong, H.
480 T., Sorooshian, A., Jonsson, H. H., Shiraiwa, M., Zuend, A., Nenes, A., Prather, K. A., Flagan,
481 R. C., & Seinfeld, J. H. (2013). Composition and hygroscopicity of the Los Angeles Aerosol:
482 CalNex. *Journal of Geophysical Research Atmospheres*, *118*(7), 3016–3036.
483 https://doi.org/10.1002/jgrd.50307

484 Hu, D., Qiao, L., Chen, J., Ye, X., Yang, X., Cheng, T., & Fang, W. (2010). Hygroscopicity of
485 inorganic aerosols: Size and relative humidity effects on the growth factor. *Aerosol and Air*
486 *Quality Research*, *10*(3), 255–264. https://doi.org/10.4209/aaqr.2009.12.0076

487 Koehler, K. A., Kreidenweis, S. M., DeMott, P. J., Petters, M. D., Prenni, A. J., & Carrico, C. M.
488 (2009). Hygroscopicity and cloud droplet activation of mineral dust aerosol. *Geophysical*
489 *Research Letters*, *36*(8), 1–5. https://doi.org/10.1029/2009GL037348

490 Laskina, O., Morris, H. S., Grandquist, J. R., Qin, Z., Stone, E. A., Tivanski, A. V., & Grassian, V. H.
491 (2015). Size Matters in the water uptake and hygroscopic growth of atmospherically relevant
492 multicomponent aerosol particles. *Journal of Physical Chemistry A*, *119*(19), 4489–4497.
493 https://doi.org/10.1021/jp510268p

494 Li, W., Teng, X., Chen, X., Liu, L., Xu, L., Zhang, J., Wang, Y., Zhang, Y., & Shi, Z. (2021). Organic
495 Coating Reduces Hygroscopic Growth of Phase-Separated Aerosol Particles. *Environmental*
496 *Science and Technology*, *55*(24), 16339–16346. https://doi.org/10.1021/acs.est.1c05901

497 Ling, T. Y., & Chan, C. K. (2008). Partial crystallization and deliquescence of particles containing
498 ammonium sulfate and dicarboxylic acids. *Journal of Geophysical Research Atmospheres*,
499 *113*(14). https://doi.org/10.1029/2008JD009779

500 Liu, P., Li, Y. J., Wang, Y., Bateman, A. P., Zhang, Y., Gong, Z., Bertram, A. K., & Martin, S. T.
501 (2018). Highly Viscous States Affect the Browning of Atmospheric Organic Particulate Matter.
502 *ACS Central Science*, *4*(2), 207–215. https://doi.org/10.1021/acscentsci.7b00452

503 Liu, P., Li, Y. J., Wang, Y., Gilles, M. K., Zaveri, R. A., Bertram, A. K., & Martin, S. T. (2016a).
504 Lability of secondary organic particulate matter. *Proceedings of the National Academy of*
505 *Sciences of the United States of America*, *113*(45), 12643–12648.
506 https://doi.org/10.1073/pnas.1603138113

507 Liu, P., Li, Y. J., Wang, Y., Gilles, M. K., Zaveri, R. A., Bertram, A. K., & Martin, S. T. (2016b).
508 Lability of secondary organic particulate matter. *Proceedings of the National Academy of*
509 *Sciences of the United States of America*, *113*(45), 12643–12648.
510 https://doi.org/10.1073/pnas.1603138113

511 Liu, P., Song, M., Zhao, T., Gunthe, S. S., Ham, S., He, Y., Qin, Y. M., Gong, Z., Amorim, J. C.,
512 Bertram, A. K., & Martin, S. T. (2018a). Resolving the mechanisms of hygroscopic growth and
513 cloud condensation nuclei activity for organic particulate matter. *Nature Communications*, *9*(1).
514 https://doi.org/10.1038/s41467-018-06622-2

515 Liu, P., Song, M., Zhao, T., Gunthe, S. S., Ham, S., He, Y., Qin, Y. M., Gong, Z., Amorim, J. C.,
516 Bertram, A. K., & Martin, S. T. (2018b). Resolving the mechanisms of hygroscopic growth and
517 cloud condensation nuclei activity for organic particulate matter. *Nature Communications*, *9*.
518 https://doi.org/10.1038/s41467-018-06622-2

519 Liu, Y. J., Zhu, T., Zhao, D. F., & Zhang, Z. F. (2008). Investigation of the hygroscopic properties of
520 Ca(NO3) 2 and internally mixed Ca(NO3)2/CaCO 3 particles by micro-Raman spectrometry.
521 *Atmospheric Chemistry and Physics*, *8*(23), 7205–7215. https://doi.org/10.5194/acp-8-7205-
522 2008

523 Liu, Y., & Laskin, A. (2009). *Hygroscopic Properties of CH3SO3Na, CH3SO3NH4, (CH3SO3)2Mg,*
524 *and (CH3SO3)2Ca Particles Studied by micro-FTIR Spectroscopy*. 1531–1538.

525 Liu, Y., Yang, Z., Desyaterik, Y., Gassman, P. L., Wang, H., & Laskin, A. (2008). Hygroscopic
526 behavior of substrate-deposited particles studied by micro-FT-IR spectroscopy and
527 complementary methods of particle analysis (Analytical Chemistry (2008) 80, (633-642)).
528 *Analytical Chemistry*, *80*(18), 7179. https://doi.org/10.1021/ac801397q

529 Marple, V. A., Rubow, K. L., & Behm, S. M. (1991). A microorifice uniform deposit impactor
530 (moudi): Description, calibration, and use. *Aerosol Science and Technology*, *14*(4), 434–436.
531 https://doi.org/10.1080/02786829108959504

532 Marple, V., Olson, B., Romay, F., Hudak, G., Geerts, S. M., & Lundgren, D. (2014). Second
533 generation micro-orifice uniform deposit impactor, 120 MOUDI-II: Design, Evaluation, and
534 application to long-term ambient sampling. *Aerosol Science and Technology*, *48*(4), 427–433.
535 https://doi.org/10.1080/02786826.2014.884274

536 Martin, S. T. (2000). Phase transitions of aqueous atmospheric particles. *Chemical Reviews*, *100*(9),
537 3403–3453. https://doi.org/10.1021/cr990034t

538 Norrish, R. (1966). Equation for the activity coefficients and equilibrium relative humidities.
539 *JInternational Journal of Food Science & Technology*, *1*, 25–39.

540 Pajunoja, A., Lambe, A. T., Hakala, J., Rastak, N., Cummings, M. J., Brogan, J. F., Hao, L.,
541 Paramonov, M., Hong, J., Prisle, N. L., Malila, J., Romakkaniemi, S., Lehtinen, K. E. J.,
542 Laaksonen, A., Kulmala, M., Massoli, P., Onasch, T. B., Donahue, N. M., Riipinen, I., …
543 Virtanen, A. (2015). Adsorptive uptake of water by semisolid secondary organic aerosols.
544 *Geophysical Research Letters*, *42*(8), 3063–3068. https://doi.org/10.1002/2015GL063142

545 Peng, C., & Chan, C. K. (2001). The water cycles of water-soluble organic salts of atmospheric
546 importance. *Atmospheric Environment*, *35*(7), 1183–1192. https://doi.org/10.1016/S1352-
547 2310(00)00426-X

548 Peng, C., Chen, L., & Tang, M. (2022). A database for deliquescence and efflorescence relative
549 humidities of compounds with atmospheric relevance. *Fundamental Research*, *2*(4), 578–587.
550 https://doi.org/10.1016/j.fmre.2021.11.021

551 Petters, M. D., & Kreidenweis, S. M. (2007). A single parameter representation of hygroscopic
552 growth and cloud condensation nucleus activity. *Atmospheric Chemistry and Physics*, *7*(8),
553 1961–1971. https://doi.org/10.5194/acp-7-1961-2007

554 Petters, M. D., Prenni, A. J., Kreidenweis, S. M., & DeMott, P. J. (2007). On measuring the critical
555 diameter of cloud condensation nuclei using mobility selected aerosol. *Aerosol Science and*
556 *Technology*, *41*(10), 907–913. https://doi.org/10.1080/02786820701557214

557 Pöhlker, M. L., Pöhlker, C., Ditas, F., Klimach, T., De Angelis, I. H., Araújo, A., Brito, J., Carbone,
558 S., Cheng, Y., Chi, X., Ditz, R., Gunthe, S. S., Kesselmeier, J., Könemann, T., Lavrič, J. V.,
559 Martin, S. T., Mikhailov, E., Moran-Zuloaga, D., Rose, D., … Pöschl, U. (2016). Long-term
560 observations of cloud condensation nuclei in the Amazon rain forest - Part 1: Aerosol size
561 distribution, hygroscopicity, and new model parametrizations for CCN prediction. *Atmospheric*
562 *Chemistry and Physics*, *16*(24), 15709–15740. https://doi.org/10.5194/acp-16-15709-2016

563 Pope, F. D., Dennis-smither, B. J., Griffiths, P. T., Clegg, S. L., & Cox, R. A. (2010). Studies of
564 Single Aerosol Particles Containing Malonic Acid, Glutaric Acid, and Their Mixtures with
565 Sodium Chloride . I . Hygroscopic Growth. *Growth Factors*, 5335–5341.

566 Prenni, A. J., Petters, M. D., Kreidenweis, S. M., DeMott, P. J., & Ziemann, P. J. (2007). Cloud
567 droplet activation of secondary organic aerosol. *Journal of Geophysical Research Atmospheres*,
568 *112*(10). https://doi.org/10.1029/2006JD007963

569 Rastak, N., Pajunoja, A., Acosta Navarro, J. C., Ma, J., Song, M., Partridge, D. G., Kirkevåg, A.,
570 Leong, Y., Hu, W. W., Taylor, N. F., Lambe, A., Cerully, K., Bougiatioti, A., Liu, P., Krejci, R.,
571 Petäjä, T., Percival, C., Davidovits, P., Worsnop, D. R., … Riipinen, I. (2017). Microphysical
572 explanation of the RH-dependent water affinity of biogenic organic aerosol and its importance
573 for climate. *Geophysical Research Letters*, *44*(10), 5167–5177.
574 https://doi.org/10.1002/2017GL073056

575 Reviakine, I., Johannsmann, D., & Richter, R. P. (2011). Hearing what you cannot see and visualizing
576 what you hear: Interpreting quartz crystal microbalance data from solvated interfaces. *Analytical*
577 *Chemistry*, *83*(23), 8838–8848. https://doi.org/10.1021/ac201778h

578 Riipinen, I., Rastak, N., & Pandis, S. N. (2015). Connecting the solubility and CCN activation of
579 complex organic aerosols: A theoretical study using solubility distributions. *Atmospheric*
580 *Chemistry and Physics*, *15*(11), 6305–6322. https://doi.org/10.5194/acp-15-6305-2015

581 Rose, D., Gunthe, S. S., Mikhailov, E., Frank, G. P., Dusek, U., Andreae, M. O., & Pöschl, U. (2008).
582 Calibration and measurement uncertainties of a continuous-flow cloud condensation nuclei
583 counter (DMT-CCNC): CCN activation of ammonium sulfate and sodium chloride aerosol
584 particles in theory and experiment. *Atmospheric Chemistry and Physics*, *8*(5), 1153–1179.
585 https://doi.org/10.5194/acp-8-1153-2008

586 Shi, J., Hong, J., Ma, N., Luo, Q., He, Y., Xu, H., Tan, H., Wang, Q., Tao, J., Zhou, Y., Han, S., Peng,
587 L., Xie, L., Zhou, G., Xu, W., Sun, Y., Cheng, Y., & Su, H. (2022). Measurement report: On the
588 difference in aerosol hygroscopicity between high and low relative humidity conditions in the
589 North China Plain. *Atmospheric Chemistry and Physics*, *22*(7), 4599–4613.
590 https://doi.org/10.5194/acp-22-4599-2022

591 Smith, M. L., Bertram, A. K., & Martin, S. T. (2012). Deliquescence, efflorescence, and phase
592 miscibility of mixed particles of ammonium sulfate and isoprene-derived secondary organic
593 material. *Atmospheric Chemistry and Physics*, *12*(20), 9613–9628. https://doi.org/10.5194/acp-
594 12-9613-2012

595 Smith, M. L., Kuwata, M., & Martin, S. T. (2011). Secondary organic material produced by the dark
596 ozonolysis of-pinene minimally affects the deliquescence and efflorescence of ammonium
597 sulfate. *Aerosol Science and Technology*, *45*(2), 244–261.
598 https://doi.org/10.1080/02786826.2010.532178

599 Smith, M. L., You, Y., Kuwata, M., Bertram, A. K., & Martin, S. T. (2013). Phase transitions and
600 phase miscibility of mixed particles of ammonium sulfate, toluene-derived secondary organic
601 material, and water. *Journal of Physical Chemistry A*, *117*(36), 8895–8906.
602 https://doi.org/10.1021/jp405095e

603 Starzak, M., & Peacock, S. D. (1997). Water activity coefficient in aqueous solutions of sucrose -a
604 comprehensive data analysis. *Zuckerindustrie*, *122*(5), 380–387.

605 Tang, M., Chan, C. K., Li, Y. J., Su, H., Ma, Q., Wu, Z., Zhang, G., Wang, Z., Ge, M., Hu, M., He,
606 H., & Wang, X. (2019). A review of experimental techniques for aerosol hygroscopicity studies.

Atmospheric Chemistry and Physics, *19*(19), 12631–12686. https://doi.org/10.5194/acp-19-12631-2019

Valsan, A. E., Ravikrishna, R., Biju, C. V., Pöhlker, C., Després, V. R., Huffman, J. A., Pöschl, U., & Gunthe, S. S. (2016). Fluorescent biological aerosol particle measurements at a tropical high-Altitude site in southern India during the southwest monsoon season. *Atmospheric Chemistry and Physics*, *16*(15), 9805–9830. https://doi.org/10.5194/acp-16-9805-2016

Wang, Y., Li, Z., Zhang, Y., Du, W., Zhang, F., Tan, H., Xu, H., Fan, T., Jin, X., Fan, X., Dong, Z., Wang, Q., & Sun, Y. (2018). Characterization of aerosol hygroscopicity, mixing state, and CCN activity at a suburban site in the central North China Plain. *Atmospheric Chemistry and Physics*, *18*(16), 11739–11752. https://doi.org/10.5194/acp-18-11739-2018

Wang, Z., Cheng, Y., Ma, N., Mikhailov, E., Pöschl, U., & Su, H. (2017). Dependence of the hygroscopicity parameter κ on particle size, humidity and solute concentration: implications for laboratory experiments, field measurements and model studies. *Atmospheric Chemistry and Physics*, *March*, 1–33. https://doi.org/10.5194/acp-2017-253

Wittbom, C., Eriksson, A. C., Rissler, J., Roldin, P., Nordin, E. Z., Sjogren, S., Nilsson, P. T., Swietlicki, E., Pagels, J., & Svenningsson, B. (2018). Effect of solubility limitation on hygroscopic growth and cloud drop activation of SOA particles produced from traffic exhausts. *Journal of Atmospheric Chemistry*, *75*(4), 359–383. https://doi.org/10.1007/s10874-018-9380-5

Wu, Z. J., Poulain, L., Henning, S., Dieckmann, K., Birmili, W., Merkel, M., Van Pinxteren, D., Spindler, G., Müller, K., Stratmann, F., Herrmann, H., & Wiedensohler, A. (2013). Relating particle hygroscopicity and CCN activity to chemical composition during the HCCT-2010 field campaign. *Atmospheric Chemistry and Physics*, *13*(16), 7983–7996. https://doi.org/10.5194/acp-13-7983-2013

Wu, Z. J., Zheng, J., Shang, D. J., Du, Z. F., Wu, Y. S., Zeng, L. M., Wiedensohler, A., & Hu, M. (2016). Particle hygroscopicity and its link to chemical composition in the urban atmosphere of Beijing, China, during summertime. *Atmospheric Chemistry and Physics*, *16*(2), 1123–1138. https://doi.org/10.5194/acp-16-1123-2016

Zhang, S., Shen, X., Sun, J., Zhang, Y., Zhang, X., Xia, C., Hu, X., Zhong, J., Wang, J., & Liu, S. (2023). Atmospheric particle hygroscopicity and the influence by oxidation state of organic aerosols in urban Beijing. *Journal of Environmental Sciences (China)*, *124*, 544–556. https://doi.org/10.1016/j.jes.2021.11.019

Zhao, P., Ge, S., Su, J., Ding, J., & Kuang, Y. (2022). Relative Humidity Dependence of Hygroscopicity Parameter of Ambient Aerosols. *Journal of Geophysical Research: Atmospheres*, *127*(8), 1–10. https://doi.org/10.1029/2021JD035647

Zieger, P., Väisänen, O., Corbin, J. C., Partridge, D. G., Bastelberger, S., Mousavi-Fard, M., Rosati, B., Gysel, M., Krieger, U. K., Leck, C., Nenes, A., Riipinen, I., Virtanen, A., & Salter, M. E. (2017a). Revising the hygroscopicity of inorganic sea salt particles. *Nature Communications*, *8*(July). https://doi.org/10.1038/ncomms15883

Zieger, P., Väisänen, O., Corbin, J. C., Partridge, D. G., Bastelberger, S., Mousavi-Fard, M., Rosati, B., Gysel, M., Krieger, U. K., Leck, C., Nenes, A., Riipinen, I., Virtanen, A., & Salter, M. E. (2017b). Revising the hygroscopicity of inorganic sea salt particles. *Nature Communications*, *8*(May). https://doi.org/10.1038/ncomms15883

649 Zobrist, B., Soonsin, V., Luo, B. P., Krieger, U. K., Marcolli, C., Peter, T., & Koop, T. (2011). Ultra-
650 slow water diffusion in aqueous sucrose glasses. *Physical Chemistry Chemical Physics*, *13*(8),
651 3514–3526. https://doi.org/10.1039/c0cp01273d

652

Figure.

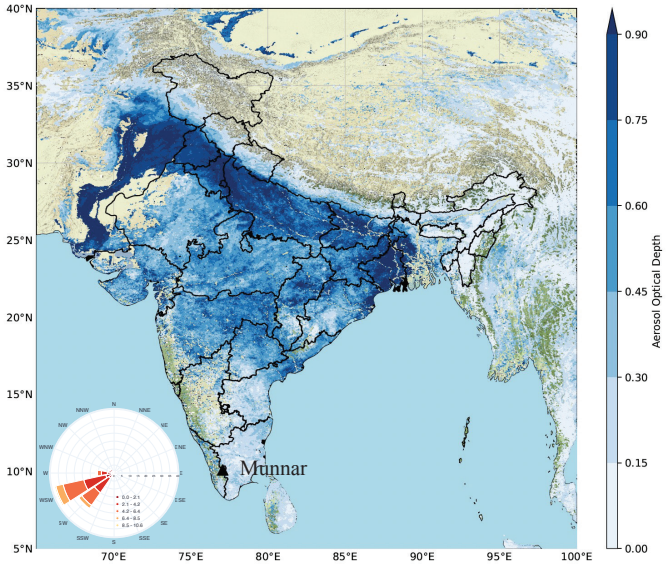

Figure 1. Spatial distribution of average Aerosol Optical Depth (AOD) derived from MODIS (Moderate Resolution Imaging Spectroradiometer) Level 2 data over the Indian continental region during the monsoon season of 2021 (June - September). The AOD distribution clearly indicates a relatively lower aerosol loading over the observational site of Munnar (marked as a black triangle) compared with the other parts of India. The wind rose diagram shown in the inset is average wind speed and wind direction arriving at the sampling site during the ambient aerosol sampling period (August – September 2021). The prevailing air masses mostly originated over the Indian Ocean and arrived from southwest direction, bringing clean marine influx to the observational site, confirming the relatively low influence of anthropogenic activities.

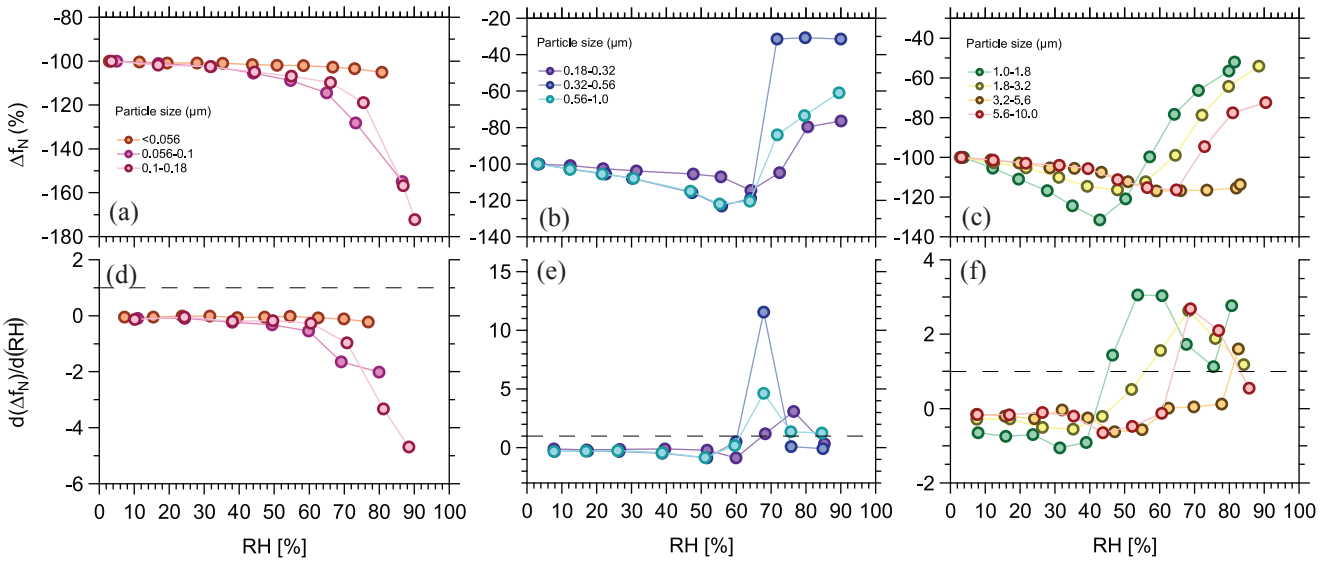

Figure 2. Deliquescence phase transition behaviour of size-resolved ambient aerosol particles from Munnar. For panels a, b, and c, Δf_N represents the change in the oscillation frequency of the quartz crystal microbalance (QCM) sensor resulting due to water uptake by the ambient aerosol particles at different relative humidity (RH) conditions normalised to that of the dry aerosol particles at RH <5%, expressed as percentage. The decrease in the value of Δf_N for each size range for the sampled ambient aerosol particles indicates the water uptake at different RH conditions in the subsaturated regime. The solid markers and lines identify different particle size ranges. In panels d, e, and f the derivative of Δf_N with respect to RH ($d(\Delta f_N)/d(RH)$) is plotted against RH to determine the deliquescence relative humidity (DRH) value corresponding to the respective aerosol size ranges. The RH values at which $d(\Delta f_N)/d(RH)$ becomes ≥1 (marked by the dotted line) represent the DRH values for the individual aerosol size ranges.

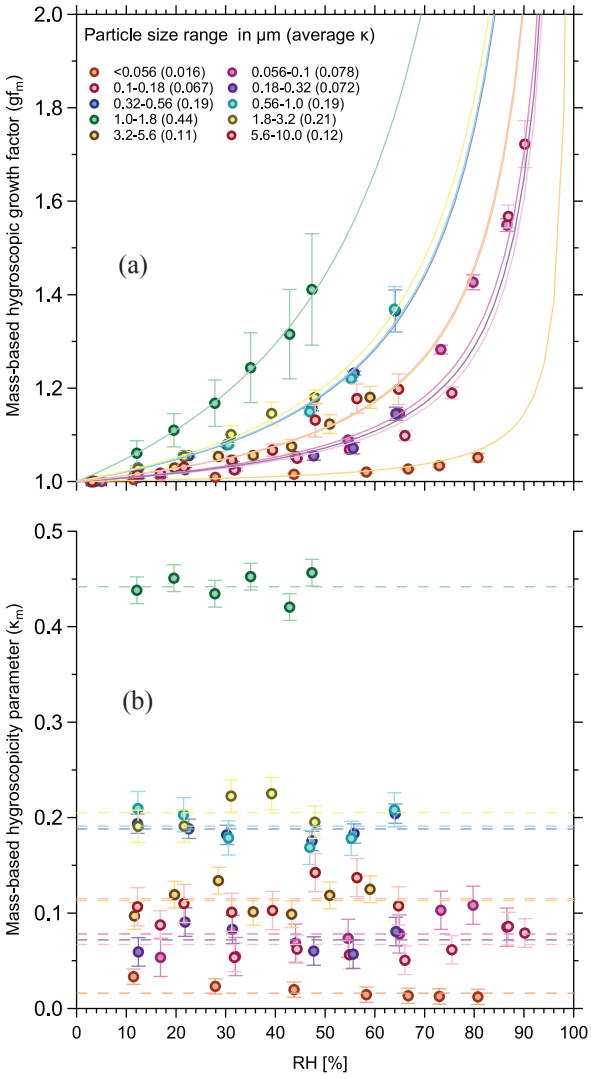

Figure 3. Size-resolved hygroscopicity measurements of ambient aerosol particles at the high-altitude site, Munnar, during the Monsoon season (August-September 2021). (a) Mass-based hygroscopic growth factor (gf_m) derived using a quartz crystal microbalance (QCM) for ten different size ranges of ambient aerosol particles at different relative humidity (RH) conditions in the subsaturated regime (circles). The solid lines represent the corresponding κ-Köhler growth factor fits obtained using the mean value of mass-based hygroscopicity parameter, κ_m. The error bars represent the variations in gf_m averaged over the mass change corresponding to different overtone frequencies of the QCM sensor at respective RH conditions. The values in parentheses are the mean κ_m values corresponding to respective size ranges. (b) The data points are the κ_m values calculated based on the gf_m (as shown in (a)) using the κ-Köhler theory for different RH conditions in the subsaturated regime. The dotted lines represent the mean κ_m value for each size range of ambient aerosol particles and the error bars represent one standard deviation.

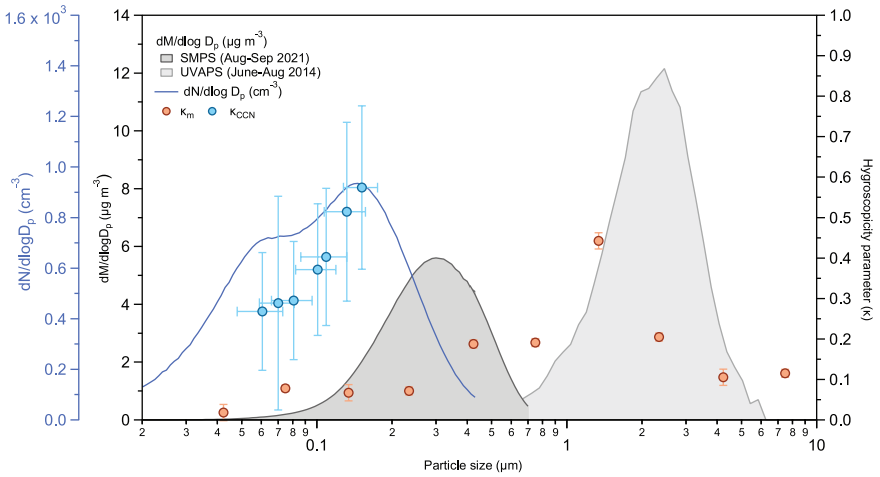

Figure 4. Aerosol size distributions, hygroscopicity parameters derived from quartz crystal microbalance (QCM) experiments (κ_m), and from size-resolved cloud condensation nuclei (CCN) measurements (κ_{CCN}). The number size distribution obtained using a Scanning Mobility Particle Sizer (SMPS) over the size range of 10 – 430 nm (blue curve) was measured during the sampling period and exhibited a bimodal distribution. The mass size distributions (dark grey shaded area) were derived based on the aerosol number size distribution by assuming a density of 1.2 g cm^{-3} for the submicron region. The mass size distribution for the supermicron range (light grey shaded area) was obtained using Ultraviolet Aerodynamic Particle Sizer (UV-APS) measurements during the same season (June-August) but for a different year (2014). The hygroscopicity parameters derived from QCM experiments (κ_m; orange points) and size-resolved CCN measurements (κ_{CCN}; blue points) are shown for the comparison. The error bars for κ_m and κ_{CCN} indicate the measurement uncertainty and variability, respectively.

Complex hygroscopic behaviour of ambient aerosol particles revealed by a piezoelectric technique

Christi Jose[1,2], Aishwarya Singh[1,2], Kavyashree N. Kalkura[1,2], George V. Jose[3], Shailina Srivastava[1,2], Rameshchand K. A.[4], Shweta Yadav[5], R. Ravikrishna[2,6], M. O. Andreae[7,8,9], Scot T. Martin[10,11], Pengfei Liu[12,*], and Sachin S. Gunthe[1,2,*]

[1]Environemntal Engineering Division, Dept of Civil Engineering, Indian Institute of Technology Madras, Chennai 600036, India

[2]Centre for Atmospheric and Climate Sciences, Indian Institute of Technology Madras, Chennai 600036, India

[3]Dept of Civil Engineering, Indian Institute of Technology Bombay, Mumbai 400076, India

[4]Dept of Mechanical Engineering, College of Engineering Munnar, Munnar 685612, India

[5]Dept of Environmental Sciences, Central University of Jammu, Samba, Jammu and Kashmir 181143, India

[6]Dept of Chemical Engineering, Indian Institute of Technology Madras, Chennai 600036, India

[7]Multiphase Chemistry Department, Max Planck Institute for Chemistry, 55128 Mainz, Germany

[8]Scripps Institution of Oceanography, University of California San Diego, La Jolla, CA 92093, USA

[9]Department of Geology and Geophysics, King Saud University, Riyadh 11451, Saudi Arabia

[10]Department of Earth and Planetary Sciences, Harvard University, Cambridge, MA 02138, USA

[11]John A. Paulson School of Engineering & Applied Sciences, Harvard University, Cambridge, MA 02138, USA

[12]School of Earth and Atmospheric Sciences, Georgia Institute of Technology, Atlanta, GA 30332, USA

*Correspondence to: Sachin S. Gunthe (s.gunthe@iitm.ac.in) and Pengfei Liu (pengfei.liu@eas.gatech.edu)

KEYPOINTS

- QCM technique revealed aerosol properties at low RH values offering insights that may not be captured by traditional size-based measurements
- The size-dependent variations in aerosol properties below DRH emphasize the need to understand how aerosol properties change with RH history
- Organic in aerosols complicate its cloud forming ability, necessitating additional studies in diverse environments to improve climate models

ABSTRACT

Comprehending the intricate interplay between atmospheric aerosols and water vapour in subsaturated regions is vital for accurate modelling of aerosol–cloud–radiation–climate dynamics. But the microphysical mechanisms governing these interactions with ambient aerosols remain inadequately understood. Here we report results from high-altitude, relatively pristine site in Western-Ghats of India during monsoon, serving as a baseline for climate processes in one of the world's most polluted regions. Utilizing a novel quartz crystal microbalance (QCM) approach, we conducted size-resolved sampling to analyse humidity-dependent growth factors, hygroscopicity, deliquescence behaviour, and aerosol liquid water content (ALWC). Fine-mode aerosols (≤2.5 μm) exhibited size-dependent interactions with water vapour, contributing significantly to ALWC. Deliquescence was observed in larger aerosols (>180 nm), influenced by organic species, with deliquescence relative humidity (DRH) lower than that of pure inorganic salts. This research highlights the significance of understanding ambient aerosol-water interactions and hygroscopicity for refining climate models in subsaturated conditions.

PLAIN LANGUAGE SUMMARY

Aerosol particles interact with water vapour in the atmosphere. Understanding these interactions in sub – and super-saturated regions is crucial because they affect processes such as cloud formation, radiation, and climate. We collected ambient aerosol samples from Western Ghats in India to understand natural processes that happen without significant human interventions. Using a special technique involving a quartz crystal sensor, we measured different aspects, such as how aerosols grow with humidity, their ability to uptake the water molecules, and when they transition from solid to liquid (deliquescence). Interestingly, fine particles, especially those smaller than 2.5 μm, exhibited unique behaviours. While larger particles underwent a transition from solid to liquid under certain conditions, this didn't happen for the smaller particles. These findings highlight the importance of understanding these interactions for more accurate climate predictions.

1. INTRODUCTION

Understanding the hygroscopicity of atmospheric aerosols is crucial for assessing cloud formation and their climate and air pollution impact (Cheung et al., 2015). Investigation of the hygroscopicity of ambient aerosols poses significant challenges due to their chemical complexity, particle size variation, phase state, and viscosity. Techniques like Fourier transform infrared spectroscopy (FTIR) (Y. Liu et al., 2008; Y. Liu & Laskin, 2009), quartz crystal microbalance (QCM) (Chao et al., 2020; Demou et al., 2003; P. Liu et al., 2016a; P. Liu, Song, et al., 2018a), Raman spectroscopy (Ling & Chan, 2008; Y. J. Liu et al., 2008), electrodynamic balance (EDB) (Choi & Chan, 2002; Peng & Chan, 2001; Pope et al., 2010), optical microscopy (OM) (Ahn et al., 2010; Eom et al., 2014; Gupta et al., 2015), hygroscopicity tandem differential mobility analysis (HTDMA) (Cheung et al., 2015; Prenni et al., 2007; Zieger et al., 2017a) and size-selected cloud condensation nuclei (CCN) spectrometry (Petters et al., 2007; Pöhlker et al., 2016; Rose et al., 2008) have been employed to study the hygroscopicity of laboratory – generated and ambient aerosols (Tang et al., 2019). However, a consensus on the most effective method is lacking, leading to inconsistent and incomparable results. Hygroscopicity measurements primarily focus on accumulation mode particles, limiting data on nucleation and coarse mode particles with complex behaviours. Discrepancies in hygroscopic properties and organic and inorganic species composition in atmospheric aerosols result in diverse growth factors and phase transitions, crucial for accurate climate modelling (Li et al., 2021).

The QCM is effective in determining mass–based hygroscopicity and physical property variations of atmospherically–relevant aerosols (Demou et al., 2003; P. Liu et al., 2016b; P. Liu, Song, et al., 2018b). It overcomes the limitations of traditional methods like HTDMA, which has a narrow particle size range with limited relative humidity (RH) resolution (Zhao et al., 2022). Conventional HTDMA methods inadequately reveal hygroscopicity heterogeneity and phase transitions in wider aerosol size range, impacting processes like CCN activation and aerosol liquid water (Li et al., 2021). QCM's mass-based measurements accurately quantify aerosol hygroscopicity behaviour across a wide RH range in the atmosphere, detailing physical property variations during phase transitions and help to delineate water uptake mechanisms, including solubility and water diffusion limitations (P. Liu, Li, et al., 2018; P. Liu, Song, et al., 2018b).

India's climate is distinct and intricate, and as per the 2020 climate change assessment report, India has faced challenges like temperature rise and extreme weather events since the mid-20th century. A key hurdle in addressing these issues is the absence of systematic aerosol characteristic measurements, particularly in aerosol-water vapor interactions in the subsaturated regime (Cheung et al., 2015). Aerosol particles from a forest-surrounded by pristine area are anticipated to contain substantial biogenic organic aerosols. The dynamic chemical transformation of secondary organic aerosols (SOA) in the atmosphere leads to intricate compositions. Atmospheric processing further complicates the understanding of phase state and properties of atmospheric aerosols (Rastak et al., 2017). In this study, QCM measurements are utilized to explore aerosol hygroscopicity dependence on RH, chemical composition, and size across a broad range of ambient aerosols in India's relatively pristine setting.

2. MATERIALS AND METHODS

Size-resolved ambient aerosols were sampled at the Natural Aerosol and Bioaerosol High Altitude (NABHA) Laboratory at the College of Engineering, Munnar (10.0930° N, 77.0682° E; 1600 m above mean sea level), a high-altitude and typically clean site situated in the Western Ghats of India, using a 10-stage micro-orifice uniform deposit impactor (MOUDI-II 120-R, TSI) (V. Marple et al., 2014; V. A. Marple et al., 1991) during the monsoon season (August-September) of 2021. Ambient particles collected on PTFE (Polytetrafluoroethylene) filters were transferred to a hydrophobic SiO_2-coated quartz sensor by gently pressing the filter paper onto the sensor. The hygroscopic growth factor, hygroscopicity parameter and deliquescence relative humidity (DRH) were estimated using a highly sensitive mass balance instrument, QCM (QSense Analyzer, Biolin Scientific) (P. Liu, Song, et al., 2018a; Reviakine et al., 2011). The accuracy and robustness of the method were demonstrated by performing measurements of the hygroscopic growth factor and DRH for sucrose and $(NH_4)_2SO_4$ particles, respectively, which were compared with previously reported results (Arenas et al., 2012a; Chao et al., 2020; Martin, 2000; Norrish, 1966; Peng et al., 2022; Starzak & Peacock, 1997; Zobrist et al., 2011) (Fig. S3 and S4). The hygroscopic growth factor and the corresponding hygroscopicity parameter, κ, were determined over a wide range of RH conditions using κ-Köhler theory (Petters & Kreidenweis, 2007), where κ represents a quantitative measure of aerosol water uptake characteristics and CCN activity (Zhao et al., 2022). The water uptake characteristics and the phase transition behaviours of the ambient

samples were investigated and compared between different size ranges of particles below 10 µm collected using the MOUDI sampler. The Aerosol Liquid Water Content (ALWC) (Bian et al., 2014) at different RH conditions was also estimated from corresponding hygroscopicity parameters for each size range of particles (Fig. S5). The number size distributions of the ambient aerosol particles of size 10 to 420 nm [measured in parallel using a scanning mobility particle sizer – SMPS, comprised of an electrostatic classifier (EC, TSI Model 3082) equipped with a differential mobility analyser (DMA, TSI Model 3081) and a condensation particle counter (CPC, TSI Model 3750)], were then converted to mass size distributions assuming a particle density of 1.2 g cm^{-3} (DeCarlo et al., 2004). The supermicron particle mass size distribution for the same season, but a different year, was used in this study, which had been obtained using an Ultraviolet Aerodynamic Particle Sizer (UV-APS, TSI Inc., model 3314) (Valsan et al., 2016).

Meteorological parameters were recorded using an automatic weather station (AWS, Clima Sensor US) during the sampling period. Figure 1 shows the sampling site – Munnar, along with aerosol optical depth (AOD) over India during the monsoon season, indicating the relatively pristine nature of the sampling site. During the measurement, airmasses predominantly arrived from the southwest direction, bringing clean marine influx to the observational site and resulting in a low influence of anthropogenic emissions (Fig. 1). A more detailed description of the instruments, experimental techniques, and estimation of various parameters is provided in the Supporting Information (SI).

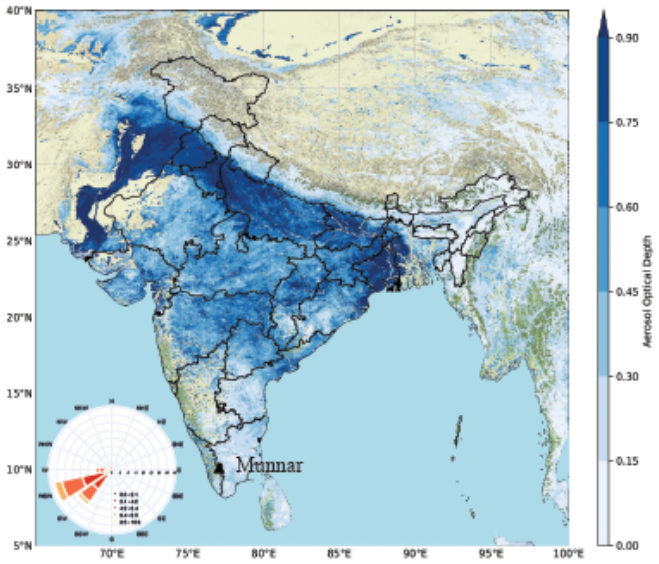

Figure 1. Spatial distribution of average Aerosol Optical Depth (AOD) derived from MODIS (Moderate Resolution Imaging Spectroradiometer) Level 2 data over the Indian continental region during the monsoon season of 2021 (June - September). The AOD distribution clearly indicates a relatively low aerosol loading over the observational site of Munnar (marked as a black triangle) compared with the other parts of India. The wind rose diagram shown in the inset shows the average wind speed and wind direction arriving at the sampling site during the ambient aerosol sampling period (August – September 2021). The prevailing air masses mostly originated over the Indian Ocean and arrived from southwest direction, bringing clean marine influx to the observational site, confirming the relatively low influence of anthropogenic activities.

3. RESULTS AND DISCUSSION

The QCM sensor's oscillation frequency variation (Δf) signifies water uptake and release, providing insights into adsorption, desorption, and physical states of particles during solid-to-aqueous phase transition (Arenas et al., 2012b). Normalizing the frequency shift at higher RH to that of deposited dry sample (RH <5%) yields the percentage value, Δf_N (Chao et al., 2020). Figure 2 shows Δf_N for the ambient aerosol particles across various RH levels and sampled size ranges. A negative sign in Δf_N indicates frequency reduction with increasing RH due to water uptake. Further details of Δf_N and its derivative, $d(\Delta f_N)/(RH)$, are available in SI.

For the particle size <180 nm (Fig. 2a), Δf_N decreased, implying water uptake, with <56 nm particles exhibiting the lowest value. In Figure 2b and 2c, particles showed increased water uptake at lower RH, evidenced by Δf_N decrease. However, Δf_N suddenly increased at specific RH, indicating a drastic water uptake leading to deliquescence-induced phase transition. Figures 2a-c revealed deliquescence in particles >180 nm at different RH (known as DRH), absent in those <180 nm. Past studies reported no deliquescence for ambient and laboratory-generated atmospherically relevant particles even at high RH, attributing them to organic nature (Arenas et al., 2012a; Brooks et al., 2002; Chao et al., 2020; Peng et al., 2022). We hypothesize that particles <180 nm were likely dominated by freshly formed secondary organic aerosols (SOA) from biogenic volatile organic compound (VOC) oxidation, supported by the densely vegetated/forest region and season. Concurrent quasi-continuous measurements during the same campaign indicated upto ~90% organic fraction in NR-PM_1 (non-refractory particulate matter with an aerodynamic diameter ≤1 μm; Tab. S2) with details discussed in subsequent studies.

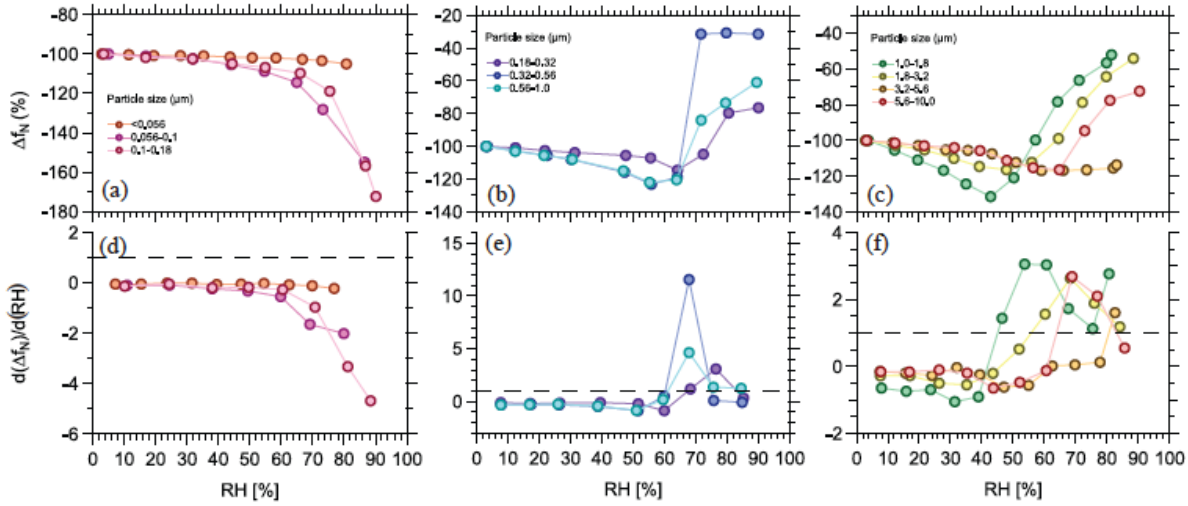

Figure 2. Deliquescence phase transition behaviour of size-resolved ambient aerosol particles from Munnar. For panels a, b, and c, Δf_N represents the change in the oscillation frequency of the quartz crystal microbalance (QCM) sensor resulting due to water uptake by the ambient aerosol particles at different relative humidity (RH) conditions normalized to that of the dry aerosol particles at RH <5%, expressed as percentage. The decrease in the value of Δf_N for each size range for the sampled ambient aerosol particles indicates the water uptake at different RH conditions in the subsaturated regime. The solid markers and lines identify different particle size ranges. In panels d, e, and f, the derivative of Δf_N with respect to RH ($d(\Delta f_N)/d(RH)$) is plotted against RH to determine the deliquescence relative humidity (DRH) value corresponding to the respective aerosol size ranges. The RH values at which $d(\Delta f_N)/d(RH)$ becomes ≥1 (marked by the dotted line) represent the DRH values for the individual aerosol size ranges.

Following Chao et al. (2020), DRH, indicated by $d(\Delta f_N)/(RH) \geq 1$ ranged from ~60 – 68% for three size ranges (180 nm – 320 nm; 320 nm – 560 nm; 560 nm – 1 µm) in this study (Fig. 2e). Above 180 nm, inorganic salts, like $(NH_4)_2SO_4$, may contribute to DRH appearance (Hu et al., 2010) (Fig. 2b,e). These DRH values, smaller than pure $(NH_4)_2SO_4$ (DRH=80%), suggest mixed salts and/or organic compounds in the sampled aerosol particles. The deliquescence behaviour of organic-inorganic mixtures introduces complexity due to solubility limitations, influenced by the organic species in the aerosol particles. Previous studies noted reduced DRH of inorganic species and sometimes, unaffected by organics (Smith et al., 2011, 2012, 2013). Thus, we hypothesize 180 nm to 1 µm particles at this site reflect a complex mixture of inorganic salts like $(NH_4)_2SO_4$ and water-soluble organic compounds. Supermicron particles (>1 µm), except 1 – 1.8 µm, showed <17% Δf_N, indicating lower water uptake (Fig. 2c). Beyond maximum water uptake, the three size ranges exhibited different DRH values. 1.8 – 3.2 µm and 5.6 – 10 µm exhibited DRH between 56 – 68%, suggesting a mixture of water-soluble organic compounds and inorganic salts. However, 3.2 – 5.6 µm showed a very high DRH (>81%) with the organic fraction minimally affecting DRH due to solubility limitations. For 1.8 – 3.2 µm and 5.6 – 10 µm, reduced DRH

compared to pure inorganic salts suggests a mix of water-soluble organic and inorganic compounds (Smith et al., 2011, 2012, 2013). The 1.0 – 1.8 μm range exhibited a >30% Δf_N reduction at ~42% RH, indicating a higher water uptake and the observed DRH appeared to be ~45 – 53%, consistent with the highest κ_m (~0.44, see discussion below) among all measured size ranges (Chao et al., 2020). The low DRH at this site suggests presence of highly water-soluble organic material within the organic-inorganic (sea salt) mixture in this size range.

Figure 3 shows the size-resolved mass-based hygroscopic growth factors (gf_m) and the corresponding mass-based hygroscopicity parameters (κ_m) of ambient aerosol particles calculated from QCM measurements (Text S4 and S5) over a wide RH range (2 – 90%). In Figure 3a, the growth factor increases with water uptake in humid air, showing size-dependent variations across different RH levels (indicated by markers). Each size range had a maximum RH limit beyond which gf_m estimation was impossible due to deliquescence, as observed in previous studies (Chao et al., 2020). Accordingly, the highest gf_m=1.72 was recorded at RH=90% for the 100 – 180 nm particles. The pronounced variations in gf_m between different-sized particles at a given RH indicate varying chemical composition and hygroscopicity across the sampled sizes.

Figure 3b shows the size-dependent average κ_m values, calculated from the gf_m values in Figure 3a. Each particle size range exhibited minimal κ_m variation (average $\kappa_m \pm 0.007$), suggesting ideal solution behaviour across the wide RH range (Z. Wang et al., 2017). The average κ_m values (indicated by dashed lines in Figure 3b) of the size-resolved ambient particles varied significantly between 0.016 (<0.056 nm) and 0.44 (1.0 – 1.8 μm) over the investigated RH range. This implies κ_m as a function of size, and indicates distinct chemical compositions for each size fraction. For example, the small increase in κ_m from 0.016 to 0.078 for particles <56 nm to 56-100 nm, respectively, is potentially owing to aging processes (Zhang et al., 2023). Aerosol particles <320 nm exhibited very low average κ_m (0.06), which may be primarily due to the strong dominance of organic compounds in these size ranges (Demou et al., 2003; Li et al., 2021; Shi et al., 2022). The particles in the size range of 320 nm – 1 μm were moderately hygroscopic (average κ_m=0.19) indicating the influence of inorganic salts (Wu et al., 2016). The particles between 1.0 – 1.8 μm exhibited highest κ_m (0.44), which implies the presence of highly hygroscopic material such as sea salt

(Zieger et al., 2017b) mixed with organic compounds. Even larger particles exhibited reduced κ_m, possibly due to the presence of dust particles (Koehler et al., 2009), transported at this site during monsoon season (Valsan et al., 2016). The κ-Köhler parameterization fit accurately elucidates the gf_m within each size range over a wide range of RH values (Petters & Kreidenweis, 2007).

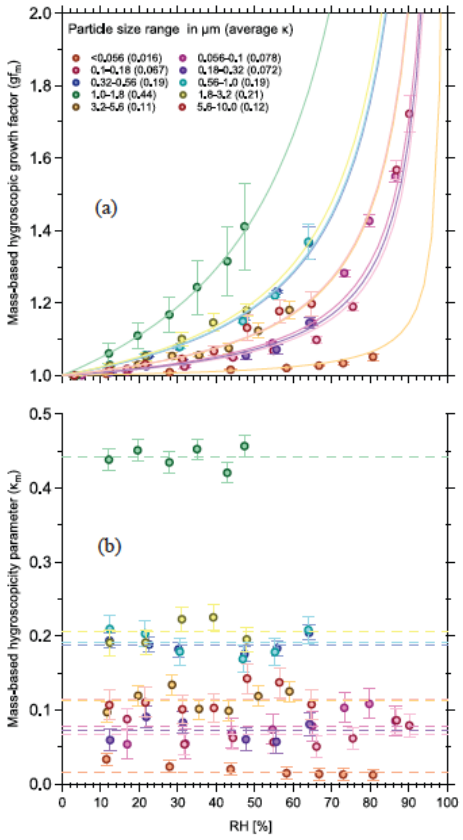

Figure 3. Size-resolved hygroscopicity measurements of ambient aerosol particles at the high-altitude site, Munnar, during the Monsoon season (August-September 2021). (a) Mass-based hygroscopic growth factor (gf_m) derived using a quartz crystal microbalance (QCM) for ten different size ranges of ambient aerosol particles at different relative humidity (RH) conditions in the subsaturated regime (circles). The solid lines represent the corresponding κ-Köhler growth factor fits obtained using the mean value of mass-based hygroscopicity parameters, κ_m. The error bars represent the variations in gf_m averaged over the mass change corresponding to different overtone frequencies of the QCM sensor at respective RH conditions. The values in parentheses are the mean κ_m values corresponding to the respective size ranges. (b) The data points are the κ_m values calculated based on the gf_m (as shown in (a)) using the κ-Köhler theory for different RH conditions in the subsaturated regime. The dotted lines represent the mean κ_m value for each size range of ambient aerosol particles and the error bars represent one standard deviation.

Figure 4 shows the size dependency of κ_m in the subsaturated regime measured by QCM together with κ_{CCN} (Text S2) in the supersaturated regime determined by size-resolved CCN measurements and aerosol size distributions obtained by SMPS and UV-APS. The submicron particles show a bimodal number size distribution with an Aitken mode peak at 63 nm and an accumulation mode at 145 nm, while the mass size distributions peak at 350 nm and 3 µm,

respectively. The average κ_{CCN} increased from a value of 0.28 for the Aitken mode particles to 0.47 for the accumulation mode particles. In the submicron region, κ_m exhibited a nominal increase with particle size (Wu et al., 2016). in parallel with the increase in κ_{CCN}, albeit at much lower absolute values. This increase likely reflects the decrease of organic fraction with size in the submicron range, which is supported by the appearance of deliquescence in the size range above 180 nm, indicating the presence of inorganic salts. In the supermicron region (for particles ≥1 μm), κ_m peaked due to the potential presence of NaCl particles in the size range 1.0 – 1.8 μm, and decreased again in the higher size ranges (>1.8 μm) likely because of the presence of dust particles. The average κ_m value (0.18) obtained from QCM measurements across all the sampled size ranges in the subsaturated regime was lower than the average κ_{CCN} (0.39), likely due to the solubility limitation (Dusek et al., 2011; Hersey et al., 2013; Rastak et al., 2017; Riipinen et al., 2015; Wittbom et al., 2018) of organic and inorganic compounds in ambient aerosol particles below the DRH. Most inorganic species are completely dissolved beyond the DRH point in the subsaturated regime, allowing κ_{CCN} to assume complete particle solubility (Pajunoja et al., 2015; Petters & Kreidenweis, 2007).

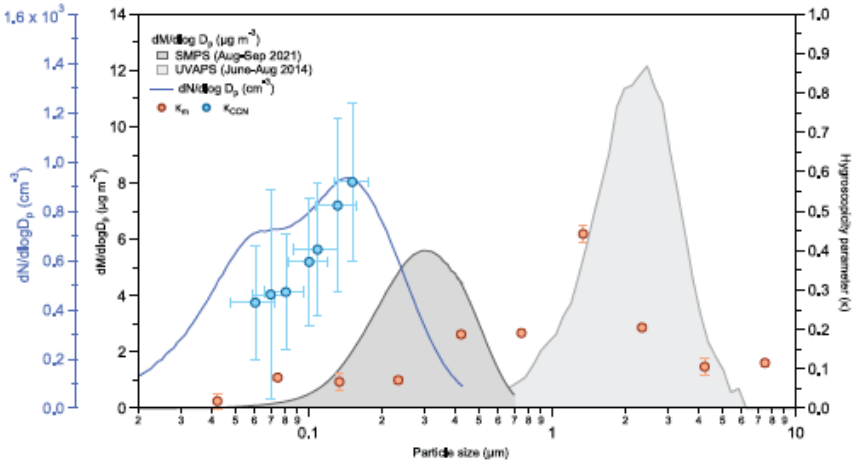

Figure 4. Aerosol size distributions, hygroscopicity parameters derived from quartz crystal microbalance (QCM) experiments (κ_m), and from size-resolved cloud condensation nuclei (CCN) measurements (κ_{CCN}). The number size distribution obtained using a Scanning Mobility Particle Sizer (SMPS) over the size range of 10 – 430 nm (blue curve) was measured during the sampling period and exhibited a bimodal distribution. The mass size distributions (dark grey shaded area) were derived based on the aerosol number size distribution by assuming a density of 1.2 g cm^{-3} for the submicron region. The mass size distribution for the supermicron range (light grey shaded area) was obtained using Ultraviolet Aerodynamic Particle Sizer (UV-APS) measurements during the same season (June-August) but for a different year (2014). The hygroscopicity parameters derived from QCM experiments (κ_m; orange points) and size-resolved CCN measurements (κ_{CCN}; blue points) are shown for the comparison. The error bars for κ_m and κ_{CCN} indicate the measurement uncertainty and variability, respectively.

Unlike QCM measurements, the hygroscopicity parameters obtained in previous studies using the HTDMA technique (κ_{HTDMA}) are often consistent with κ_{CCN}, as the particle

hygroscopicity is determined by particle size increase above DRH point, unaffected by solubility limits (Pajunoja et al., 2015; Y. Wang et al., 2018; Wu et al., 2013). The technical limitations, particularly limited diameter changes corresponding to gf_m values less than 2.0, prevent HTDMA from measuring aerosol hygroscopic properties below the DRH point in the subsaturated regime (Laskina et al., 2015). In contrast, the QCM technique, which is not subject to these limitations, can be used to understand the water uptake characteristics of aerosol particles in the subsaturated regime below DRH and substantially enhance our understanding about solubility limitations of organic and inorganic compounds in the lower RH region. Such an enhancement in the knowledge is crucial for accurately quantifying the radiative forcing effects of ambient aerosol particles in the atmosphere. The strong size dependence of κ_m also indicated varying chemical composition for different size ranges measured in this study.

4. SUMMARY AND ATMOSPHERIC IMPLICATIONS

We report the first results based on a high-sensitivity QCM technique to investigate the mass-based growth factor and hygroscopicity parameter of size–resolved ambient aerosols over a wide range of RH from a relatively pristine high–altitude site in India. For the investigated size ranges, the pronounced variations in gf_m below the DRH provided an opportunity to better understand the changes in ambient aerosol properties even at low RH values, which may not be revealed by size-based growth factor measurements (Hu et al., 2010; Laskina et al., 2015). These measurements clearly highlight the important and critical role in knowing the changes in aerosol properties based on their RH history for an improved understanding of water uptake, phase transition, and radiative impact of atmospheric aerosol particles (Zhao et al., 2022). Based on the estimated κ_m values, the ambient aerosol particles exhibited the behaviour of an ideal solution (Pajunoja et al., 2015) and strong size-dependent chemical composition. We further observed a pronounced size dependency of the DRH values potentially resulting from complexities of organic solubility in organic–inorganic mixtures (Li et al., 2021). Such a complexity owing to the presence of various organic species may alter the CCN behaviour of atmospheric aerosol particles due to phase transitions and changes in physical properties. The understanding of CCN activation in the supersaturated regime under the assumption of complete solubility of particles is relatively well established. But the understanding of the thermodynamic properties associated with particle growth in the subsaturated regime still remains a challenge. Our findings emphasize the need for additional experiments on ambient and atmospherically relevant laboratory-generated aerosol particles

using high-sensitivity techniques like QCM. We demonstrated the importance of this technique to better understand the rapid changes in aerosol properties resulting from exposure to a wide range of atmospheric RH conditions. The enhancement in our understanding of the complex interplay between water vapour and aerosol particles will help in developing more accurate models to effectively describe the role of aerosols in atmospheric processes to reduce climate uncertainties and assess the impact of air pollution on human and ecosystem health.

ASSOCIATED CONTENT

Author contributions

SSG conceived the idea. SSG and PL conceptualized the study and designed the research. CJ further developed and validated the QCM measurements for the ambient aerosol studies. CJ performed the field measurement campaign to collect the aerosol samples with support from AS, KNK, and RKA. CJ performed all the laboratory experiments using QCM with support from SS. GVJ performed the satellite data analysis to obtain the AOD values. CJ carried out the data analysis obtained from QCM with input from PL and SSG. CJ and AS performed the scientific interpretation of the QCM data under the mentorship of RR, SSG and PL. CJ wrote the first draft of manuscript under the mentorship of SSG with inputs from PL and RR, and further edits from SY. MOA and STM further provided critical and valuable inputs on the manuscript.

Open research

The data used in the manuscript has been deposited in an open research repository as Excel files, accessible at https://doi.org/10.6084/m9.figshare.24512377. MODIS data were sourced from the Level 2 and Atmosphere Archive and Distribution System (LAADS) (https://doi.org/10.5067/MODIS/MYD04_3K.061). Figures were prepared using Igor Pro version 9 (WaveMetrics Inc.), licensed by SSG and accessible at https://www.wavemetrics.com/software/igor-pro-9.

Acknowledgments

SSG gratefully acknowledges funding from the Ministry of Earth Sciences (MoES; sanction number MoES/16/20/12-RDEAS dated 31. Mar.2014), Government of India, for the purchase of the Cloud Condensation Nuclei Counter (CCNc). This work was supported by partial funding from the Ministry of Earth Sciences (MoES; sanction number MoES/16/04/2017-APHH (PROMOTE)), the Government of India, and the Department of Science and Technology (sanction number DST/CCP/CoE/141/2018C), the Government of India for the purchase of Quartz Crystal Microbalance (QCM). PL acknowledges the start-up funding support from the Georgia Institute of Technology. CJ acknowledges the Department of Science and Technology, the Government of India for the fellowship. Authors acknowledge the valuable support and help provided by the staff at the College of Engineering Munnar during the campaign, with special and critical help from Jyothish Jose. CJ acknowledges the

428 invaluable assistance provided by Emil Varghese during the laboratory experiments. We are
429 thankful to the support staff from Biolin Scientific, and Specialise Instruments Marketing
430 Company, Mumbai, India for their help during the experiments. We acknowledge the
431 National Aeronautics and Space Administration (NASA) for making Moderate Resolution
432 Imaging Spectroradiometer (MODIS) Earth data available to the user community.

References

Ahn, K. H., Kim, S. M., Jung, H. J., Lee, M. J., Eom, H. J., Maskey, S., & Ro, C. U. (2010). Combined use of optical and electron microscopic techniques for the measurement of hygroscopic property, chemical composition, and morphology of individual aerosol particles. *Analytical Chemistry*, *82*(19), 7999–8009. https://doi.org/10.1021/ac101432y

Arenas, K. J. L., Schill, S. R., Malla, A., & Hudson, P. K. (2012a). Deliquescence phase transition measurements by quartz crystal microbalance frequency shifts. *Journal of Physical Chemistry A*, *116*(29), 7658–7667. https://doi.org/10.1021/jp3016722

Arenas, K. J. L., Schill, S. R., Malla, A., & Hudson, P. K. (2012b). Deliquescence phase transition measurements by quartz crystal microbalance frequency shifts. *Journal of Physical Chemistry A*, *116*(29), 7658–7667. https://doi.org/10.1021/jp3016722

Bian, Y. X., Zhao, C. S., Ma, N., Chen, J., & Xu, W. Y. (2014). A study of aerosol liquid water content based on hygroscopicity measurements at high relative humidity in the North China Plain. *Atmospheric Chemistry and Physics*, *14*(12), 6417–6426. https://doi.org/10.5194/acp-14-6417-2014

Brooks, S. D., Wise, M. E., Cushing, M., & Tolbert, M. A. (2002). Deliquescence behavior of organic/ammonium sulfate aerosol. *Geophysical Research Letters*, *29*(19). https://doi.org/10.1029/2002GL014733

Chao, H. J., Huang, W. C., Chen, C. L., Chou, C. C. K., & Hung, H. M. (2020). Water Adsorption vs Phase Transition of Aerosols Monitored by a Quartz Crystal Microbalance. *ACS Omega*, *5*(49), 31858–31866. https://doi.org/10.1021/acsomega.0c04698

Cheung, H. H. Y., Yeung, M. C., Li, Y. J., Lee, B. P., & Chan, C. K. (2015). Relative Humidity-Dependent HTDMA Measurements of Ambient Aerosols at the HKUST Supersite in Hong Kong, China. *Aerosol Science and Technology*, *49*(8), 643–654. https://doi.org/10.1080/02786826.2015.1058482

Choi, M. Y., & Chan, C. K. (2002). The effects of organic species on the hygroscopic behaviors of inorganic aerosols. *Environmental Science and Technology*, *36*(11), 2422–2428. https://doi.org/10.1021/es0113293

DeCarlo, P. F., Slowik, J. G., Worsnop, D. R., Davidovits, P., & Jimenez, J. L. (2004). Particle morphology and density characterization by combined mobility and aerodynamic diameter measurements. Part 1: Theory. *Aerosol Science and Technology*, *38*(12), 1185–1205. https://doi.org/10.1080/027868290903907

Demou, E., Visram, H., Donaldson, D. J., & Makar, P. A. (2003). Uptake of water by organic films: The dependence on the film oxidation state. *Atmospheric Environment*, *37*(25), 3529–3537. https://doi.org/10.1016/S1352-2310(03)00430-8

Dusek, U., Frank, G. P., Massling, A., Zeromskiene, K., Iinuma, Y., Schmid, O., Helas, G., Hennig, T., Wiedensohler, A., & Andreae, M. O. (2011). Water uptake by biomass burning aerosol at sub-and supersaturated conditions: Closure studies and implications for the role of organics. *Atmospheric Chemistry and Physics*, *11*(18), 9519–9532. https://doi.org/10.5194/acp-11-9519-2011

Eom, H. J., Gupta, D., Li, X., Jung, H. J., Kim, H., & Ro, C. U. (2014). Influence of collecting substrates on the characterization of hygroscopic properties of inorganic aerosol particles. *Analytical Chemistry*, *86*(5), 2648–2656. https://doi.org/10.1021/ac4042075

476 Gupta, D., Kim, H., Park, G., Li, X., Eom, H. J., & Ro, C. U. (2015). Hygroscopic properties of NaCl
477 and NaNO3 mixture particles as reacted inorganic sea-salt aerosol surrogates. *Atmospheric*
478 *Chemistry and Physics*, *15*(6), 3379–3393. https://doi.org/10.5194/acp-15-3379-2015

479 Hersey, S. P., Craven, J. S., Metcalf, A. R., Lin, J., Lathem, T., Suski, K. J., Cahill, J. F., Duong, H.
480 T., Sorooshian, A., Jonsson, H. H., Shiraiwa, M., Zuend, A., Nenes, A., Prather, K. A., Flagan,
481 R. C., & Seinfeld, J. H. (2013). Composition and hygroscopicity of the Los Angeles Aerosol:
482 CalNex. *Journal of Geophysical Research Atmospheres*, *118*(7), 3016–3036.
483 https://doi.org/10.1002/jgrd.50307

484 Hu, D., Qiao, L., Chen, J., Ye, X., Yang, X., Cheng, T., & Fang, W. (2010). Hygroscopicity of
485 inorganic aerosols: Size and relative humidity effects on the growth factor. *Aerosol and Air*
486 *Quality Research*, *10*(3), 255–264. https://doi.org/10.4209/aaqr.2009.12.0076

487 Koehler, K. A., Kreidenweis, S. M., DeMott, P. J., Petters, M. D., Prenni, A. J., & Carrico, C. M.
488 (2009). Hygroscopicity and cloud droplet activation of mineral dust aerosol. *Geophysical*
489 *Research Letters*, *36*(8), 1–5. https://doi.org/10.1029/2009GL037348

490 Laskina, O., Morris, H. S., Grandquist, J. R., Qin, Z., Stone, E. A., Tivanski, A. V., & Grassian, V. H.
491 (2015). Size Matters in the water uptake and hygroscopic growth of atmospherically relevant
492 multicomponent aerosol particles. *Journal of Physical Chemistry A*, *119*(19), 4489–4497.
493 https://doi.org/10.1021/jp510268p

494 Li, W., Teng, X., Chen, X., Liu, L., Xu, L., Zhang, J., Wang, Y., Zhang, Y., & Shi, Z. (2021). Organic
495 Coating Reduces Hygroscopic Growth of Phase-Separated Aerosol Particles. *Environmental*
496 *Science and Technology*, *55*(24), 16339–16346. https://doi.org/10.1021/acs.est.1c05901

497 Ling, T. Y., & Chan, C. K. (2008). Partial crystallization and deliquescence of particles containing
498 ammonium sulfate and dicarboxylic acids. *Journal of Geophysical Research Atmospheres*,
499 *113*(14). https://doi.org/10.1029/2008JD009779

500 Liu, P., Li, Y. J., Wang, Y., Bateman, A. P., Zhang, Y., Gong, Z., Bertram, A. K., & Martin, S. T.
501 (2018). Highly Viscous States Affect the Browning of Atmospheric Organic Particulate Matter.
502 *ACS Central Science*, *4*(2), 207–215. https://doi.org/10.1021/acscentsci.7b00452

503 Liu, P., Li, Y. J., Wang, Y., Gilles, M. K., Zaveri, R. A., Bertram, A. K., & Martin, S. T. (2016a).
504 Lability of secondary organic particulate matter. *Proceedings of the National Academy of*
505 *Sciences of the United States of America*, *113*(45), 12643–12648.
506 https://doi.org/10.1073/pnas.1603138113

507 Liu, P., Li, Y. J., Wang, Y., Gilles, M. K., Zaveri, R. A., Bertram, A. K., & Martin, S. T. (2016b).
508 Lability of secondary organic particulate matter. *Proceedings of the National Academy of*
509 *Sciences of the United States of America*, *113*(45), 12643–12648.
510 https://doi.org/10.1073/pnas.1603138113

511 Liu, P., Song, M., Zhao, T., Gunthe, S. S., Ham, S., He, Y., Qin, Y. M., Gong, Z., Amorim, J. C.,
512 Bertram, A. K., & Martin, S. T. (2018a). Resolving the mechanisms of hygroscopic growth and
513 cloud condensation nuclei activity for organic particulate matter. *Nature Communications*, *9*(1).
514 https://doi.org/10.1038/s41467-018-06622-2

515 Liu, P., Song, M., Zhao, T., Gunthe, S. S., Ham, S., He, Y., Qin, Y. M., Gong, Z., Amorim, J. C.,
516 Bertram, A. K., & Martin, S. T. (2018b). Resolving the mechanisms of hygroscopic growth and
517 cloud condensation nuclei activity for organic particulate matter. *Nature Communications*, *9*.
518 https://doi.org/10.1038/s41467-018-06622-2

519 Liu, Y. J., Zhu, T., Zhao, D. F., & Zhang, Z. F. (2008). Investigation of the hygroscopic properties of
520 Ca(NO3) 2 and internally mixed Ca(NO3)2/CaCO 3 particles by micro-Raman spectrometry.
521 *Atmospheric Chemistry and Physics*, *8*(23), 7205–7215. https://doi.org/10.5194/acp-8-7205-
522 2008

523 Liu, Y., & Laskin, A. (2009). *Hygroscopic Properties of CH3SO3Na, CH3SO3NH4, (CH3SO3)2Mg,*
524 *and (CH3SO3)2Ca Particles Studied by micro-FTIR Spectroscopy*. 1531–1538.

525 Liu, Y., Yang, Z., Desyaterik, Y., Gassman, P. L., Wang, H., & Laskin, A. (2008). Hygroscopic
526 behavior of substrate-deposited particles studied by micro-FT-IR spectroscopy and
527 complementary methods of particle analysis (Analytical Chemistry (2008) 80, (633-642)).
528 *Analytical Chemistry*, *80*(18), 7179. https://doi.org/10.1021/ac801397q

529 Marple, V. A., Rubow, K. L., & Behm, S. M. (1991). A microorifice uniform deposit impactor
530 (moudi): Description, calibration, and use. *Aerosol Science and Technology*, *14*(4), 434–436.
531 https://doi.org/10.1080/02786829108959504

532 Marple, V., Olson, B., Romay, F., Hudak, G., Geerts, S. M., & Lundgren, D. (2014). Second
533 generation micro-orifice uniform deposit impactor, 120 MOUDI-II: Design, Evaluation, and
534 application to long-term ambient sampling. *Aerosol Science and Technology*, *48*(4), 427–433.
535 https://doi.org/10.1080/02786826.2014.884274

536 Martin, S. T. (2000). Phase transitions of aqueous atmospheric particles. *Chemical Reviews*, *100*(9),
537 3403–3453. https://doi.org/10.1021/cr990034t

538 Norrish, R. (1966). Equation for the activity coefficients and equilibrium relative humidities.
539 *JInternational Journal of Food Science & Technology*, *1*, 25–39.

540 Pajunoja, A., Lambe, A. T., Hakala, J., Rastak, N., Cummings, M. J., Brogan, J. F., Hao, L.,
541 Paramonov, M., Hong, J., Prisle, N. L., Malila, J., Romakkaniemi, S., Lehtinen, K. E. J.,
542 Laaksonen, A., Kulmala, M., Massoli, P., Onasch, T. B., Donahue, N. M., Riipinen, I., …
543 Virtanen, A. (2015). Adsorptive uptake of water by semisolid secondary organic aerosols.
544 *Geophysical Research Letters*, *42*(8), 3063–3068. https://doi.org/10.1002/2015GL063142

545 Peng, C., & Chan, C. K. (2001). The water cycles of water-soluble organic salts of atmospheric
546 importance. *Atmospheric Environment*, *35*(7), 1183–1192. https://doi.org/10.1016/S1352-
547 2310(00)00426-X

548 Peng, C., Chen, L., & Tang, M. (2022). A database for deliquescence and efflorescence relative
549 humidities of compounds with atmospheric relevance. *Fundamental Research*, *2*(4), 578–587.
550 https://doi.org/10.1016/j.fmre.2021.11.021

551 Petters, M. D., & Kreidenweis, S. M. (2007). A single parameter representation of hygroscopic
552 growth and cloud condensation nucleus activity. *Atmospheric Chemistry and Physics*, *7*(8),
553 1961–1971. https://doi.org/10.5194/acp-7-1961-2007

554 Petters, M. D., Prenni, A. J., Kreidenweis, S. M., & DeMott, P. J. (2007). On measuring the critical
555 diameter of cloud condensation nuclei using mobility selected aerosol. *Aerosol Science and*
556 *Technology*, *41*(10), 907–913. https://doi.org/10.1080/02786820701557214

557 Pöhlker, M. L., Pöhlker, C., Ditas, F., Klimach, T., De Angelis, I. H., Araújo, A., Brito, J., Carbone,
558 S., Cheng, Y., Chi, X., Ditz, R., Gunthe, S. S., Kesselmeier, J., Könemann, T., Lavrič, J. V.,
559 Martin, S. T., Mikhailov, E., Moran-Zuloaga, D., Rose, D., … Pöschl, U. (2016). Long-term
560 observations of cloud condensation nuclei in the Amazon rain forest - Part 1: Aerosol size
561 distribution, hygroscopicity, and new model parametrizations for CCN prediction. *Atmospheric*
562 *Chemistry and Physics*, *16*(24), 15709–15740. https://doi.org/10.5194/acp-16-15709-2016

563 Pope, F. D., Dennis-smither, B. J., Griffiths, P. T., Clegg, S. L., & Cox, R. A. (2010). Studies of
564 Single Aerosol Particles Containing Malonic Acid, Glutaric Acid, and Their Mixtures with
565 Sodium Chloride . I . Hygroscopic Growth. *Growth Factors*, 5335–5341.

566 Prenni, A. J., Petters, M. D., Kreidenweis, S. M., DeMott, P. J., & Ziemann, P. J. (2007). Cloud
567 droplet activation of secondary organic aerosol. *Journal of Geophysical Research Atmospheres*,
568 *112*(10). https://doi.org/10.1029/2006JD007963

569 Rastak, N., Pajunoja, A., Acosta Navarro, J. C., Ma, J., Song, M., Partridge, D. G., Kirkevåg, A.,
570 Leong, Y., Hu, W. W., Taylor, N. F., Lambe, A., Cerully, K., Bougiatioti, A., Liu, P., Krejci, R.,
571 Petäjä, T., Percival, C., Davidovits, P., Worsnop, D. R., … Riipinen, I. (2017). Microphysical
572 explanation of the RH-dependent water affinity of biogenic organic aerosol and its importance
573 for climate. *Geophysical Research Letters*, *44*(10), 5167–5177.
574 https://doi.org/10.1002/2017GL073056

575 Reviakine, I., Johannsmann, D., & Richter, R. P. (2011). Hearing what you cannot see and visualizing
576 what you hear: Interpreting quartz crystal microbalance data from solvated interfaces. *Analytical*
577 *Chemistry*, *83*(23), 8838–8848. https://doi.org/10.1021/ac201778h

578 Riipinen, I., Rastak, N., & Pandis, S. N. (2015). Connecting the solubility and CCN activation of
579 complex organic aerosols: A theoretical study using solubility distributions. *Atmospheric*
580 *Chemistry and Physics*, *15*(11), 6305–6322. https://doi.org/10.5194/acp-15-6305-2015

581 Rose, D., Gunthe, S. S., Mikhailov, E., Frank, G. P., Dusek, U., Andreae, M. O., & Pöschl, U. (2008).
582 Calibration and measurement uncertainties of a continuous-flow cloud condensation nuclei
583 counter (DMT-CCNC): CCN activation of ammonium sulfate and sodium chloride aerosol
584 particles in theory and experiment. *Atmospheric Chemistry and Physics*, *8*(5), 1153–1179.
585 https://doi.org/10.5194/acp-8-1153-2008

586 Shi, J., Hong, J., Ma, N., Luo, Q., He, Y., Xu, H., Tan, H., Wang, Q., Tao, J., Zhou, Y., Han, S., Peng,
587 L., Xie, L., Zhou, G., Xu, W., Sun, Y., Cheng, Y., & Su, H. (2022). Measurement report: On the
588 difference in aerosol hygroscopicity between high and low relative humidity conditions in the
589 North China Plain. *Atmospheric Chemistry and Physics*, *22*(7), 4599–4613.
590 https://doi.org/10.5194/acp-22-4599-2022

591 Smith, M. L., Bertram, A. K., & Martin, S. T. (2012). Deliquescence, efflorescence, and phase
592 miscibility of mixed particles of ammonium sulfate and isoprene-derived secondary organic
593 material. *Atmospheric Chemistry and Physics*, *12*(20), 9613–9628. https://doi.org/10.5194/acp-
594 12-9613-2012

595 Smith, M. L., Kuwata, M., & Martin, S. T. (2011). Secondary organic material produced by the dark
596 ozonolysis of-pinene minimally affects the deliquescence and efflorescence of ammonium
597 sulfate. *Aerosol Science and Technology*, *45*(2), 244–261.
598 https://doi.org/10.1080/02786826.2010.532178

599 Smith, M. L., You, Y., Kuwata, M., Bertram, A. K., & Martin, S. T. (2013). Phase transitions and
600 phase miscibility of mixed particles of ammonium sulfate, toluene-derived secondary organic
601 material, and water. *Journal of Physical Chemistry A*, *117*(36), 8895–8906.
602 https://doi.org/10.1021/jp405095e

603 Starzak, M., & Peacock, S. D. (1997). Water activity coefficient in aqueous solutions of sucrose -a
604 comprehensive data analysis. *Zuckerindustrie*, *122*(5), 380–387.

605 Tang, M., Chan, C. K., Li, Y. J., Su, H., Ma, Q., Wu, Z., Zhang, G., Wang, Z., Ge, M., Hu, M., He,
606 H., & Wang, X. (2019). A review of experimental techniques for aerosol hygroscopicity studies.

Atmospheric Chemistry and Physics, *19*(19), 12631–12686. https://doi.org/10.5194/acp-19-12631-2019

Valsan, A. E., Ravikrishna, R., Biju, C. V., Pöhlker, C., Després, V. R., Huffman, J. A., Pöschl, U., & Gunthe, S. S. (2016). Fluorescent biological aerosol particle measurements at a tropical high-Altitude site in southern India during the southwest monsoon season. *Atmospheric Chemistry and Physics*, *16*(15), 9805–9830. https://doi.org/10.5194/acp-16-9805-2016

Wang, Y., Li, Z., Zhang, Y., Du, W., Zhang, F., Tan, H., Xu, H., Fan, T., Jin, X., Fan, X., Dong, Z., Wang, Q., & Sun, Y. (2018). Characterization of aerosol hygroscopicity, mixing state, and CCN activity at a suburban site in the central North China Plain. *Atmospheric Chemistry and Physics*, *18*(16), 11739–11752. https://doi.org/10.5194/acp-18-11739-2018

Wang, Z., Cheng, Y., Ma, N., Mikhailov, E., Pöschl, U., & Su, H. (2017). Dependence of the hygroscopicity parameter κ on particle size, humidity and solute concentration: implications for laboratory experiments, field measurements and model studies. *Atmospheric Chemistry and Physics*, *March*, 1–33. https://doi.org/10.5194/acp-2017-253

Wittbom, C., Eriksson, A. C., Rissler, J., Roldin, P., Nordin, E. Z., Sjogren, S., Nilsson, P. T., Swietlicki, E., Pagels, J., & Svenningsson, B. (2018). Effect of solubility limitation on hygroscopic growth and cloud drop activation of SOA particles produced from traffic exhausts. *Journal of Atmospheric Chemistry*, *75*(4), 359–383. https://doi.org/10.1007/s10874-018-9380-5

Wu, Z. J., Poulain, L., Henning, S., Dieckmann, K., Birmili, W., Merkel, M., Van Pinxteren, D., Spindler, G., Müller, K., Stratmann, F., Herrmann, H., & Wiedensohler, A. (2013). Relating particle hygroscopicity and CCN activity to chemical composition during the HCCT-2010 field campaign. *Atmospheric Chemistry and Physics*, *13*(16), 7983–7996. https://doi.org/10.5194/acp-13-7983-2013

Wu, Z. J., Zheng, J., Shang, D. J., Du, Z. F., Wu, Y. S., Zeng, L. M., Wiedensohler, A., & Hu, M. (2016). Particle hygroscopicity and its link to chemical composition in the urban atmosphere of Beijing, China, during summertime. *Atmospheric Chemistry and Physics*, *16*(2), 1123–1138. https://doi.org/10.5194/acp-16-1123-2016

Zhang, S., Shen, X., Sun, J., Zhang, Y., Zhang, X., Xia, C., Hu, X., Zhong, J., Wang, J., & Liu, S. (2023). Atmospheric particle hygroscopicity and the influence by oxidation state of organic aerosols in urban Beijing. *Journal of Environmental Sciences (China)*, *124*, 544–556. https://doi.org/10.1016/j.jes.2021.11.019

Zhao, P., Ge, S., Su, J., Ding, J., & Kuang, Y. (2022). Relative Humidity Dependence of Hygroscopicity Parameter of Ambient Aerosols. *Journal of Geophysical Research: Atmospheres*, *127*(8), 1–10. https://doi.org/10.1029/2021JD035647

Zieger, P., Väisänen, O., Corbin, J. C., Partridge, D. G., Bastelberger, S., Mousavi-Fard, M., Rosati, B., Gysel, M., Krieger, U. K., Leck, C., Nenes, A., Riipinen, I., Virtanen, A., & Salter, M. E. (2017a). Revising the hygroscopicity of inorganic sea salt particles. *Nature Communications*, *8*(July). https://doi.org/10.1038/ncomms15883

Zieger, P., Väisänen, O., Corbin, J. C., Partridge, D. G., Bastelberger, S., Mousavi-Fard, M., Rosati, B., Gysel, M., Krieger, U. K., Leck, C., Nenes, A., Riipinen, I., Virtanen, A., & Salter, M. E. (2017b). Revising the hygroscopicity of inorganic sea salt particles. *Nature Communications*, *8*(May). https://doi.org/10.1038/ncomms15883

649 Zobrist, B., Soonsin, V., Luo, B. P., Krieger, U. K., Marcolli, C., Peter, T., & Koop, T. (2011). Ultra-
650 slow water diffusion in aqueous sucrose glasses. *Physical Chemistry Chemical Physics*, *13*(8),
651 3514–3526. https://doi.org/10.1039/c0cp01273d

652

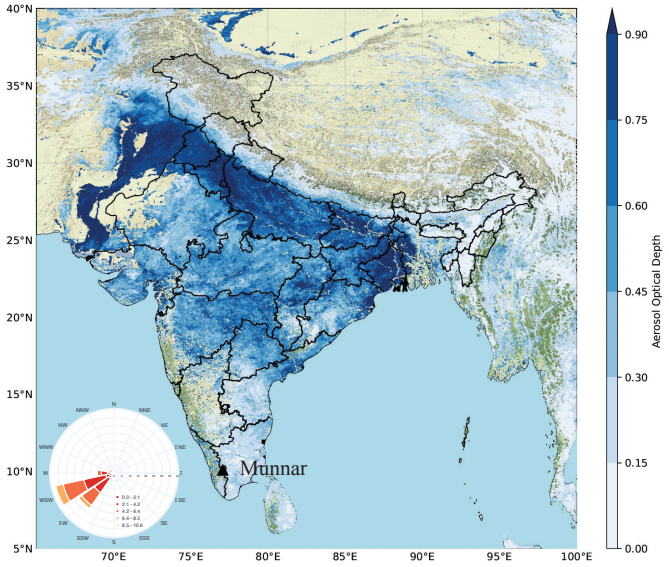

Figure 1. Spatial distribution of average Aerosol Optical Depth (AOD) derived from MODIS (Moderate Resolution Imaging Spectroradiometer) Level 2 data over the Indian continental region during the monsoon season of 2021 (June - September). The AOD distribution clearly indicates a relatively lower aerosol loading over the observational site of Munnar (marked as a black triangle) compared with the other parts of India. The wind rose diagram shown in the inset is average wind speed and wind direction arriving at the sampling site during the ambient aerosol sampling period (August – September 2021). The prevailing air masses mostly originated over the Indian Ocean and arrived from southwest direction, bringing clean marine influx to the observational site, confirming the relatively low influence of anthropogenic activities.

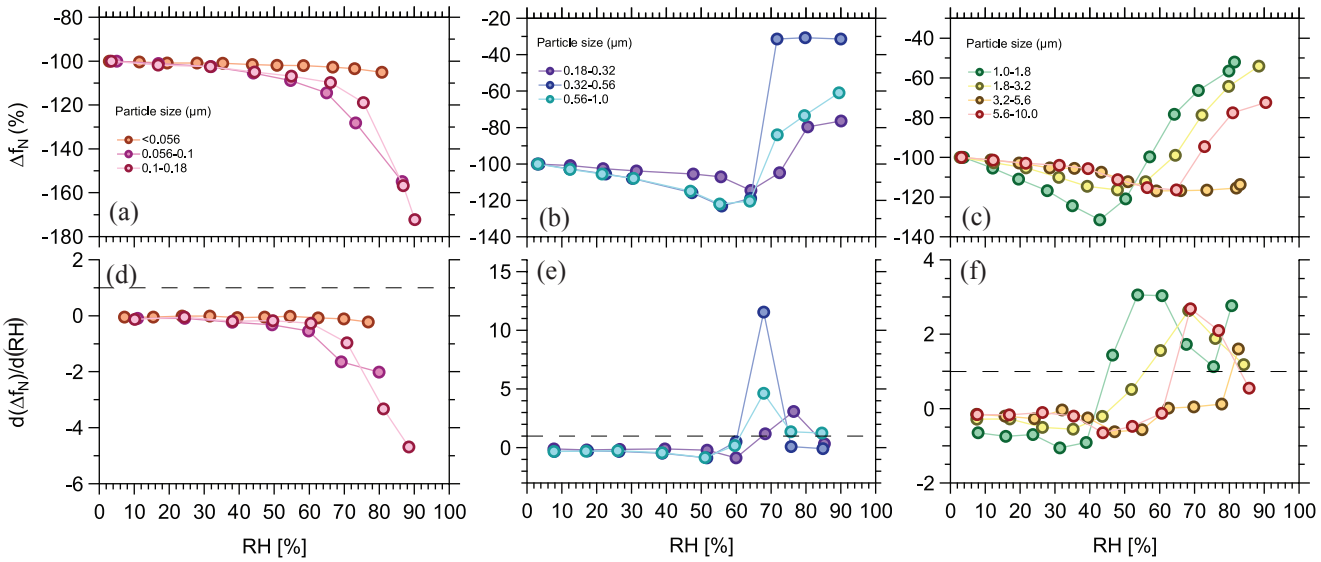

Figure 2. Deliquescence phase transition behaviour of size-resolved ambient aerosol particles from Munnar. For panels a, b, and c, Δf_N represents the change in the oscillation frequency of the quartz crystal microbalance (QCM) sensor resulting due to water uptake by the ambient aerosol particles at different relative humidity (RH) conditions normalised to that of the dry aerosol particles at RH <5%, expressed as percentage. The decrease in the value of Δf_N for each size range for the sampled ambient aerosol particles indicates the water uptake at different RH conditions in the subsaturated regime. The solid markers and lines identify different particle size ranges. In panels d, e, and f the derivative of Δf_N with respect to RH ($d(\Delta f_N)/d(RH)$) is plotted against RH to determine the deliquescence relative humidity (DRH) value corresponding to the respective aerosol size ranges. The RH values at which $d(\Delta f_N)/d(RH)$ becomes ≥1 (marked by the dotted line) represent the DRH values for the individual aerosol size ranges.

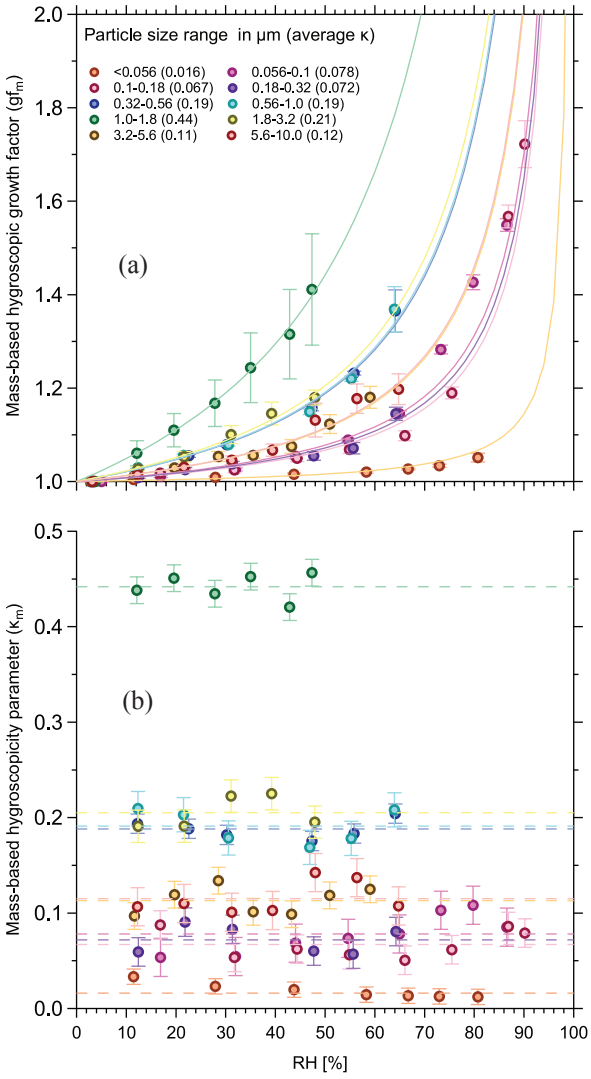

Figure 3. Size-resolved hygroscopicity measurements of ambient aerosol particles at the high-altitude site, Munnar, during the Monsoon season (August-September 2021). (a) Mass-based hygroscopic growth factor (gf_m) derived using a quartz crystal microbalance (QCM) for ten different size ranges of ambient aerosol particles at different relative humidity (RH) conditions in the subsaturated regime (circles). The solid lines represent the corresponding κ-Köhler growth factor fits obtained using the mean value of mass-based hygroscopicity parameter, κ_m. The error bars represent the variations in gf_m averaged over the mass change corresponding to different overtone frequencies of the QCM sensor at respective RH conditions. The values in parentheses are the mean κ_m values corresponding to respective size ranges. (b) The data points are the κ_m values calculated based on the gf_m (as shown in (a)) using the κ-Köhler theory for different RH conditions in the subsaturated regime. The dotted lines represent the mean κ_m value for each size range of ambient aerosol particles and the error bars represent one standard deviation.

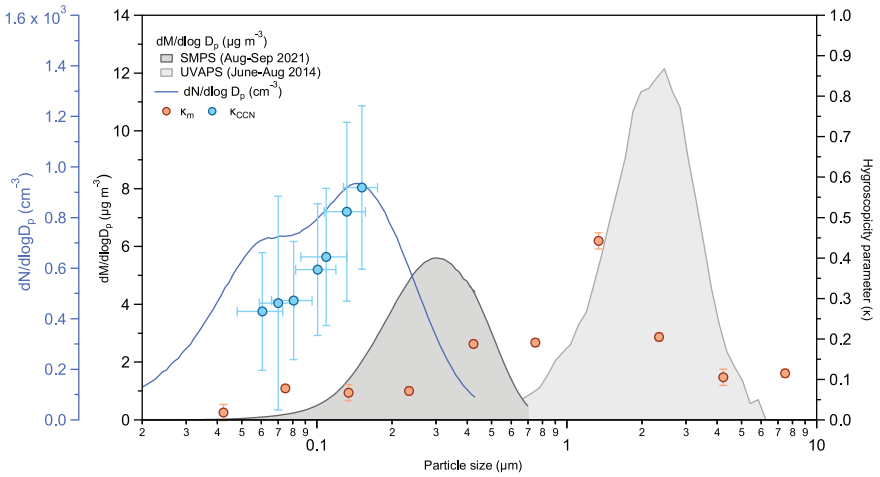

Figure 4. Aerosol size distributions, hygroscopicity parameters derived from quartz crystal microbalance (QCM) experiments (κ_m), and from size-resolved cloud condensation nuclei (CCN) measurements (κ_{CCN}). The number size distribution obtained using a Scanning Mobility Particle Sizer (SMPS) over the size range of 10 – 430 nm (blue curve) was measured during the sampling period and exhibited a bimodal distribution. The mass size distributions (dark grey shaded area) were derived based on the aerosol number size distribution by assuming a density of 1.2 g cm^{-3} for the submicron region. The mass size distribution for the supermicron range (light grey shaded area) was obtained using Ultraviolet Aerodynamic Particle Sizer (UV-APS) measurements during the same season (June-August) but for a different year (2014). The hygroscopicity parameters derived from QCM experiments (κ_m; orange points) and size-resolved CCN measurements (κ_{CCN}; blue points) are shown for the comparison. The error bars for κ_m and κ_{CCN} indicate the measurement uncertainty and variability, respectively.

Supporting Information

Complex hygroscopic behaviour of ambient aerosol particles revealed by a piezoelectric technique

Christi Jose[1,2], Aishwarya Singh[1,2], Kavyashree N. Kalkura[1,2], George V. Jose[3], Shailina Srivastava[1,2], Rameshchand K. A.[4], Shweta Yadav[5], R. Ravikrishna[2,6], M. O. Andreae[7,8,9], Scot T. Martin[10,11], Pengfei Liu[12,*], and Sachin S. Gunthe[1,2,*]

[1]Environemntal Engineering Division, Dept of Civil Engineering, Indian Institute of Technology Madras, Chennai 600036, India

[2]Centre for Atmospheric and Climate Sciences, Indian Institute of Technology Madras, Chennai 600036, India

[3]Dept of Civil Engineering, Indian Institute of Technology Bombay, Mumbai 400076, India

[4]Dept of Mechanical Engineering, College of Engineering Munnar, Munnar 685612, India

[5]Dept of Environmental Sciences, Central University of Jammu, Samba, Jammu and Kashmir 181143, India

[6]Dept of Chemical Engineering, Indian Institute of Technology Madras, Chennai 600036, India

[7]Multiphase Chemistry Department, Max Planck Institute for Chemistry, 55128 Mainz, Germany

[8]Scripps Institution of Oceanography, University of California San Diego, La Jolla, CA 92093, USA

[9]Department of Geology and Geophysics, King Saud University, Riyadh 11451, Saudi Arabia

[10]Department of Earth and Planetary Sciences, Harvard University, Cambridge, MA 02138, USA

[11]John A. Paulson School of Engineering & Applied Sciences, Harvard University, Cambridge, MA 02138, USA

[12]School of Earth and Atmospheric Sciences, Georgia Institute of Technology, Atlanta, GA 30332, USA

*Correspondence to: Sachin S. Gunthe (s.gunthe@iitm.ac.in) and Pengfei Liu (pengfei.liu@eas.gatech.edu)

List of supporting materials:

1. Seven texts, Text S1 - Text S7
2. Two tables, Table S1 – Table S2
3. Five figures, Figure S1 – Figure S5
4. References

Text S1. Sampling Site

The sampling was conducted at the Natural Aerosol and Bioaerosol High Altitude (NABHA) Laboratory at the College of Engineering, Munnar (10.0930° N, 77.0682° E), located in the Western Ghats of India, one of the most significant biodiversity hotspots in the world (Kale et al., 2016). The site is at about ~1600 m in elevation and 90 km from the Arabian Sea. Munnar possesses a moderately rugged topography with high mountain peaks and deep river valleys covered with diversified vegetated areas, tea plantations, barren land/rocky areas, and water bodies (Gupta et al., 2020). During the southwest monsoon season (June-September), the Western Ghats block the south-westerly winds, causing rainfall on these mountain ranges.

Text S2. Instrumentation

The ambient aerosols were collected on polytetrafluoroethylene (PTFE) membrane filters (pore size 0.2 μm) using a Micro-Orifice Uniform Deposit Impactor (MOUDI) with a sampling flow rate of 30 L/min. The MOUDI-II 120R (TSI) utilized 10 rotating stages to achieve a uniform deposit of particles on the filters, with nominal cut-off points at 0.056, 0.10, 0.18, 0.32, 0.56, 1.0, 1.8, 3.2, 5.6, and 10 μm (Marple et al., 2014). Concurrently, various meteorological parameters such as temperature, humidity, pressure, wind speed, wind direction, and precipitation were recorded using an Automatic Weather Station (AWS, Clima Sensor US) at the sampling location throughout the sampling period.

The number size distribution of the ambient aerosol particles was measured using a Scanning Mobility Particle Sizer (SMPS), which comprises a 3082 Electrostatic Classifier with 3081 Long Differential Mobility Analyzer (L-DMA, TSI Model 3081) and a butanol-Condensation Particle Counter (CPC, TSI Model 3750). The measurements were carried out with an aerosol flow rate of 1 L/min, spanning a size range of 10.2 – 430 nm. The aerosol mass distribution measurements for the larger-sized particles (0.3 – 20.0 μm) obtained using an Ultraviolet Aerodynamic Particle Sizer (UV-APS, TSI Inc., Model 3314) from a campaign conducted at

the same location during the Monsoon season of 2014 (June-August) were also incorporated in the study.

The hygroscopicity of aerosol particles was analyzed using a sensitive mass-balance Quartz Crystal Microbalance (QCM, QSense Analyzer, Biolin Scientific), which can measure the mass changes at the nanograms level. In 1959, Sauerbrey proposed that an adsorbed mass (Δm) causes a decrease in the resonant frequency (Δf) of the quartz crystal, and their linear relationship is given by,

$$\Delta f = -\frac{C}{n}\Delta m \quad \text{(S1)}$$

where C (=17.7 ng.cm^{-2}.Hz^{-1} for 5 MHz AT-cut crystals) is the mass sensitivity constant specific to the quartz resonator and n (=1,3,5,…) is the overtone number (Sauerbrey, 1959). The Sauerbrey equation is valid only when the film deposited on the QCM quartz sensor is rigid and perfectly coupled to the sensor surface (Rodahl & Kasemo, 1995). QCM experiments were performed with a 5 MHz AT-cut quartz sensor coated with SiO_2, and the particles were uniformly deposited on the sensor. The ambient aerosol particles collected on PTFE filters were directly transferred to the QCM sensor by placing the filter on the sensor and then gently pressing it using a cotton piece. The particles on the sensor were examined under the microscope to ensure the uniformity of the film.

The relative humidity (RH) was incrementally increased from 2% to 93% to promote the uptake of water by aerosol particles, resulting in a corresponding increase in mass. The QCM provides the fundamental frequencies corresponding to the mass deposited on the sensor. Measurements were taken at various RH points in the sub-saturated region for a blank sensor and a sensor coated with aerosol particles. The difference in the frequencies between the coated and the blank sensor at a particular RH was subsequently converted to the mass of water absorbed or adsorbed at that point using the Sauerbrey equation.

The effective particle hygroscopicity, κ_{CCN} (Petters & Kreidenweis, 2007) under supersaturated conditions was determined using size-resolved Cloud Condensation Nuclei (CCN) measurements acquired through a CCN counter (CCNC, CCN-100, DMT), employing the method outlined in Rose et al. (2008).

Text S3. Experimental setup

The schematic experimental setup designed to measure the hygroscopicity of the aerosol particles using QCM is depicted in Figure S1. Dry nitrogen was passed through a HEPA filter (Whatman 6702-9500 HEPA-CAP filters) and divided into two channels, one of which was humidified using a water bubbler. Desired RH values were created by controlling the flow ratio of dry and humidified air from both channels using digital mass flow controllers (MFCs) (Alicat Scientific–50 SCCM). The RH was continuously monitored at various points in the flow pathway using thermohydrometers (testo 605i). The accuracy of the RH values in the ranges 10-35%, 35-65%, 65-90% and <10% or >90% are ±3.0%, ±2.0%, ±3.0% and ±5%, respectively. Each humidity condition was sustained until an equilibrium condition was reached, where no further evaporation and condensation happened. The amount of water absorbed by the particles at different values of RH in the sub-saturated region was measured continuously by the QCM. The QCM module temperature was kept at least 0.5 °C higher than the room temperature to avoid condensation of water vapour onto the particles inside the QCM module. The experimental setup employed a low flow range of 0-50 sccm, and any variations in the flow could significantly affect the experimental results. To mitigate this issue, the flow rate was checked at various control points before and after each experiment using a Gilibrator (Sensidyne).

To ensure accurate measurements, it is crucial to properly clean the sensor surface before depositing the particles. The sensors were cleaned with milli-Q water and methanol, then dried with N_2 gas. Subsequently, a UV-Ozone treatment was applied to eliminate various contaminants, particularly organic compounds, from the SiO_2-coated sensor. The treatment was done for 20 minutes at a power of 1 mW/cm^2 immediately before depositing the sample particles on the sensor.

Text S4. Mass-based hygroscopic growth factor (gf_m) for laboratory-generated particles

The QCM technique for determining hygroscopicity was validated for a sucrose thin film. The mass-based hygroscopic growth factor (gf_m, mass ratio of the film at an elevated RH to that at <5% RH) for sucrose particles for a range of RH (2-93%) was calculated from QCM measurements, and the results were compared with the models for testing the accuracy of the method (Liu et al., 2018).

The steps followed for making a sucrose thin film on the sensor are as follows.

1. Prepared different concentrations (0.05%, 0.15, 0.25%, 0.5% etc) of sucrose solution by dissolving sucrose in milli-Q water.

2. Cleaned the sensor surface using Milli-Q water and methanol and treated with UV-Ozone for 20 minutes.

3. The desired volume of the solution was pipetted onto the sensor surface, which was placed on a clean petriplate.

4. The sensor was then placed inside a muffle furnace with a preset temperature of 80°C for 20 minutes to remove water.

5. The sensor with the film was viewed under a microscope (Dino-Lite Edge) to analyze the uniformity of the film.

6. The sensor with a thin film of sucrose was then mounted inside one of the modules of the QCM analyzer.

7. Dry air was allowed to pass over the film for 10-12 hours to further remove the moisture content in the particles.

After checking the uniformity of the film and the stability of different overtones using QSoft software (Fig. S2), the experiment was started with a preset program in FlowVision (software that helps to control the flow rates at the MFCs). The flow rates were changed accordingly in the two MFCs for creating different humidity values starting from dry conditions (<5% RH) to a maximum of 93% RH.

The hygroscopic growth factor values obtained from the QCM measurements were in good agreement with the literature (Norrish, 1966; Starzak & Peacock, 1997; Zobrist et al., 2011) (Fig. S3).

Text S5. Mass-based hygroscopicity parameter (κ_m) for ambient aerosol particles

After transferring the aerosol particles from the filters to the sensor, the sensor was mounted inside the QCM module and the RH was incrementally increased to investigate the water uptake behavior of particles under varying humidity conditions.

We calculated the mass-based hygroscopicity parameter, κ_m, which measures the aerosol particles' ability to take up atmospheric moisture, from the growth factor values obtained from the QCM results (Petters & Kreidenweis, 2007).

$$\kappa_m = \left(\frac{1}{a_w} - 1\right)(gf_m - 1) \quad \text{(S2)}$$

where a_w is the water activity and gf_m is the mass-based growth factor of the particle at different RH values. The a_w was approximated as the fractional RH under equilibrium conditions. κ_m could be converted to a volume-based hygroscopicity parameter κ_v, using the following relationship.

$$\kappa_v = \kappa_m \times \frac{\rho_d}{\rho_w} \quad \text{(S4)}$$

where ρ_d is the effective density of the dry particle and ρ_w is the density of water (Mikhailov et al., 2013).

The experiment was repeated for the aerosol particles from different stages of MOUDI to carry out a size-resolved study. In this study, the ambient particles were solid and rigid until they deliquesce at higher RH conditions. The QCM can measure the mass of the particles under different RH conditions till they reach the phase transition point (deliquescence relative humidity, DRH).

Text S6. Estimation of Deliquescence Relative Humidity (DRH) and Aerosol Liquid Water Content (ALWC)

The phase transition behavior of ambient aerosols was investigated by analyzing the QCM frequency response curves. During the humidification cycle, the DRH point is identified as the RH at which the oscillation frequencies of QCM response start increasing upon the addition of water (Arenas et al., 2012; Chao et al., 2020). A percentage value, Δf_N, is obtained by normalizing the oscillation frequency change induced by the aerosol particles at a given RH (Δf_R) to the oscillation frequency change resulting from a dry sample (Δf_S at RH <5%) (Chao et al., 2020).

$$\Delta f_N = \left(\frac{\Delta f_R}{\Delta f_S}\right) \times (-100)\% \quad \text{(S4)}$$

The negative sign indicates that the oscillation frequency of the sensor decreases when RH increases due to water uptake by the aerosol particles. Δf_N and its derivative with respect to the measured RH, $d(\Delta f_N)/d(RH)$ were plotted for different size ranges of ambient aerosol samples (Fig. 3). The deliquescence of the particles is indicated by an increase in Δf_N or a positive value of $d(\Delta f_N)/d(RH)$. The RH at which $d(\Delta f_N)/d(RH) \geq 1$ is considered as the DRH point for the respective sample (Chao et al., 2020). Following this method, the DRH for $(NH_4)_2SO_4$ particles was estimated between 76-80% from the QCM measurements (Fig. S4), which agrees with the literature values (Arenas et al., 2012; Martin, 2000; Peng et al., 2022).

Similarly, the DRH values for size-resolved ambient aerosol particles from Munnar were estimated.

Aerosol Liquid Water Content (ALWC) at different RH conditions were also estimated from the size-resolved hygroscopic growth factor values combined with the particle number size distribution (PNSD) measurements, assuming volume conservation during the aerosol hygroscopic process (Bian et al., 2014).

$$ALWC = \left[\frac{\pi}{6}\sum_i N_i D_{d,i}^3 (gf(D_d, RH)^3 - 1)\right]\rho_W \quad \text{(S5)}$$

where N_i represents the number concentration of dry particles of the *i* th bin obtained from SMPS and UV-APS measurements, $D_{d,i}$ is the particle diameter, and ρ_W is the density of water.

Text S7. Correction for the RH values inside the QCM module

The flow rate of humidified air in the setup can be impacted by temperature instabilities, potentially affecting the results. To prevent water vapor condensation, it is crucial to maintain the QCM module temperature at a level equal to or higher than the room temperature. To account for any temperature changes inside the QCM module, the RH was corrected using the Clausius-Clapeyron equation.

$$ln\frac{P_1}{P_2} = \frac{\Delta H_{vap}}{R}\left(\frac{1}{T_2} - \frac{1}{T_1}\right) \quad \text{(S6)}$$

where P_1 and P_2 are the vapor pressures at two temperatures, T_1 and T_2, ΔH_{vap} is the enthalpy (heat) of vaporization, and R is the gas constant (8.3145 J mol^{-1} K^{-1}). The actual RH value was determined by computing the ratio of actual vapor pressure to saturation vapor pressure, expressed as a percentage.

Table S1. Mass-based hygroscopic growth factor (gf_m) and the corresponding hygroscopicity parameter (κ_m) at different RH values in the subsaturated region for different size ranges of ambient aerosol particles (<10 μm) sampled from Munnar using MOUDI. The measurements were obtained from the QCM experiments.

Particle size range (μm)											
<0.056				0.056-0.1				0.1-0.18			
RH (%)	gf_m	κ_m	κ_v	RH (%)	gf_m	κ_m	κ_v	RH (%)	gf_m	κ_m	κ_v
2.87	1.000			5.02	1.000			3.45	1.000		
11.47	1.004	0.033	0.040	16.90	1.011	0.054	0.064	16.86	1.018	0.088	0.105
27.93	1.009	0.008	0.010	31.96	1.026	0.055	0.065	31.77	1.025	0.054	0.064
43.74	1.015	0.020	0.024	44.03	1.054	0.069	0.082	44.37	1.050	0.062	0.075
58.31	1.020	0.014	0.017	54.65	1.089	0.074	0.088	54.88	1.068	0.056	0.067
66.73	1.027	0.013	0.016	64.93	1.145	0.078	0.094	66.04	1.098	0.051	0.061
72.97	1.034	0.013	0.015	73.29	1.282	0.103	0.124	75.49	1.189	0.062	0.074
80.74	1.051	0.012	0.015	79.76	1.426	0.108	0.130	90.15	1.722	0.079	0.095
				86.56	1.549	0.085	0.102	86.85	1.567	0.086	0.103

Particle size range (μm)											
0.18-0.32				0.32-0.56				0.56-1.0			
RH (%)	gf_m	κ_m	κ_v	RH (%)	gf_m	κ_m	κ_v	RH (%)	gf_m	κ_m	κ_v
2.95	1.000			3.47	1.000			3.09	1.000		
12.42	1.008	0.059	0.071	12.26	1.027	0.194	0.232	12.34	1.030	0.210	0.251
21.84	1.025	0.090	0.109	22.58	1.055	0.188	0.226	21.50	1.056	0.203	0.244
31.36	1.038	0.083	0.099	30.21	1.079	0.182	0.218	30.57	1.079	0.179	0.214
47.70	1.055	0.060	0.072	47.33	1.158	0.175	0.211	46.91	1.149	0.169	0.203
55.62	1.071	0.057	0.068	55.83	1.232	0.183	0.220	55.25	1.220	0.178	0.214
64.23	1.145	0.081	0.097	64.13	1.365	0.204	0.245	63.93	1.369	0.208	0.250

Particle size range (μm)											
1.0-1.8				1.8-3.2				3.2-5.6			
RH (%)	gf_m	κ_m	κ_v	RH (%)	gf_m	κ_m	κ_v	RH (%)	gf_m	κ_m	κ_v
3.74	1.000			2.80	1.000			3.33	1.000		
12.14	1.061	0.438	0.526	12.39	1.027	0.191	0.229	11.63	1.013	0.097	0.116
19.58	1.110	0.451	0.541	21.64	1.053	0.191	0.229	19.70	1.029	0.119	0.143
27.80	1.167	0.435	0.522	31.09	1.100	0.223	0.267	28.52	1.053	0.134	0.161
35.00	1.244	0.452	0.543	39.25	1.145	0.225	0.270	35.55	1.056	0.101	0.121
42.85	1.315	0.421	0.505	47.91	1.180	0.195	0.234	43.24	1.075	0.099	0.119
47.37	1.411	0.457	0.548					50.94	1.123	0.119	0.142
								59.05	1.180	0.125	0.150

Particle size range (μm)			
5.6-10.0			
RH (%)	gf_m	κ_m	κ_v
3.14	1.000		
12.25	1.015	0.107	0.128
21.61	1.030	0.110	0.132
31.22	1.046	0.101	0.121
39.43	1.067	0.103	0.123
48.00	1.131	0.142	0.171
56.41	1.177	0.137	0.164
64.77	1.198	0.108	0.129

Table S2. The average mass concentration (μg m^{-3}) and the mass fraction of the chemical species in NR-PM_1 measured by aerosol chemical speciation monitor (ACSM) during the period from 06.06.2021 to 27.07.2021.

NR-PM_1 Species	**Mass concentration (μg m^{-3})**	**Mass fraction**
Organics	1.15	0.50
Sulphate	0.79	0.35
Nitrate	0.08	0.04
Ammonium	0.22	0.09
Chloride	0.04	0.02

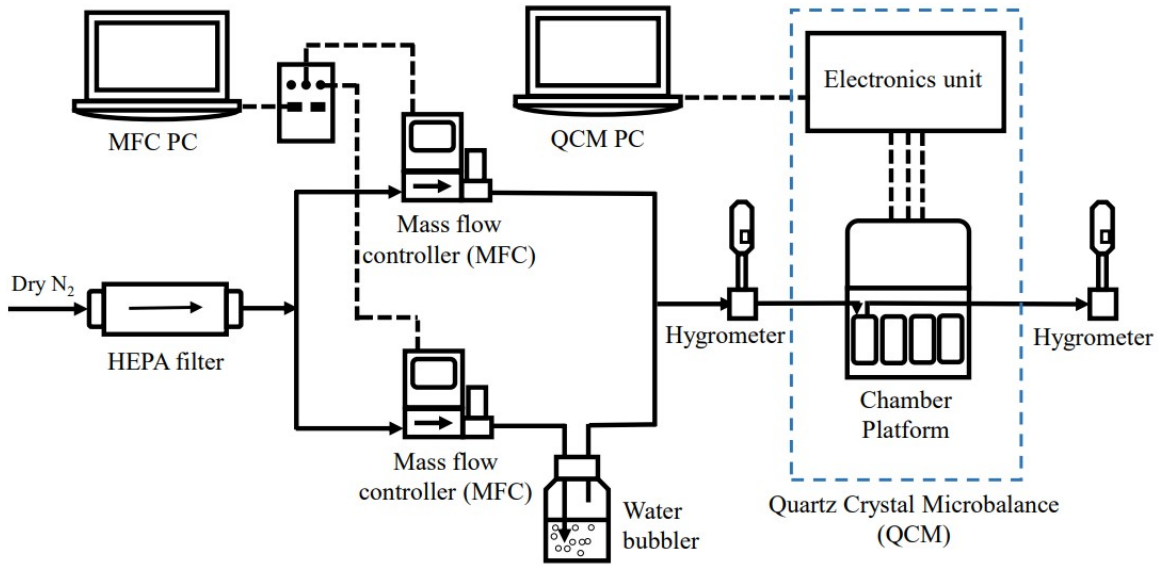

Figure S1. Schematic diagram of the experimental setup for providing a wide range of humidity conditions (2-93%) to study the aerosol-water vapor interactions of the samples coated on the quartz crystal microbalance (QCM) sensor mounted inside the module of the chamber platform. Different humidity conditions were created over the aerosol particles by controlling the flowrates of dry and humidified air using the two mass flow controllers (MFCs) connected in parallel. The RH of incoming and outgoing air is measured using two thermohygrometers connected before and after the QCM chamber platform.

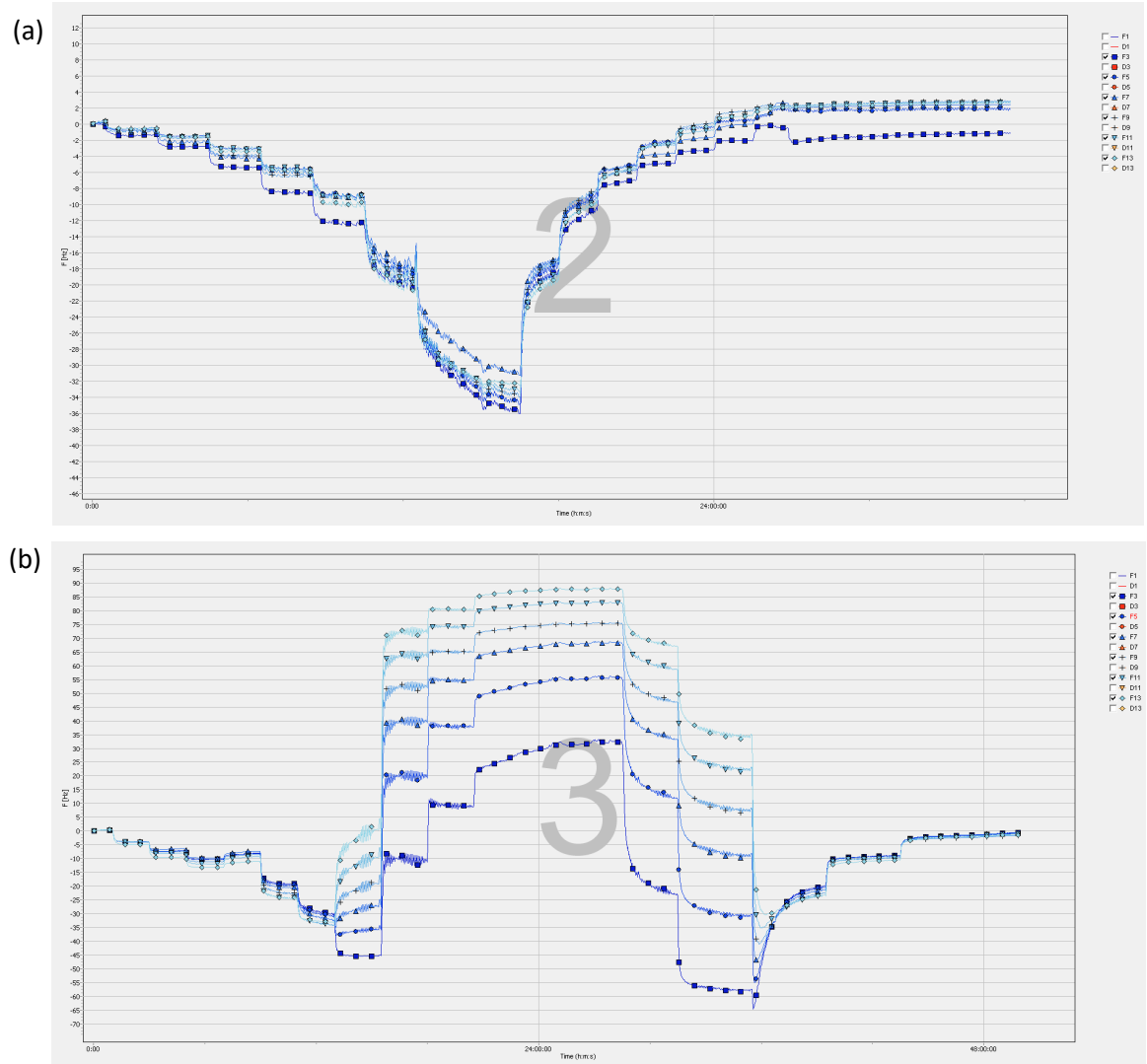

Figure S2. The screenshot of the QSoft software showing the oscillation frequency changes of the quartz crystal microbalance (QCM) sensor with time during the humidifying and drying phase of a QCM experiment for the size ranges 56-100 nm and 560 nm-1 µm of ambient aerosol particles from Munnar. (a) shows a decrease in the oscillation frequency change for the particles in the size range 56-100 nm, corresponding to an increase in mass due to water uptake during the humidifying (increasing RH) phase and a further increase in the frequency change when the water content is removed during the drying (decreasing RH) phase. (b) shows an initial decrease in the frequency change due to water uptake by the aerosol particles in the size range 560 nm-1 µm in the lower RH region (<61.2%) during the humidification cycle. The increase in frequency changes and the separation of overtones at RH=61.2% in the humidifying phase indicate that the particles undergo phase transition (deliquescence) at high RH region and become aqueous droplets leading to less viscous and non-rigid particles on the sensor. The initial frequency change value corresponding to the dry particle mass is obtained after the humidification and drying phase, indicating no particle loss. Different curves correspond to different overtone frequencies of the sensor.

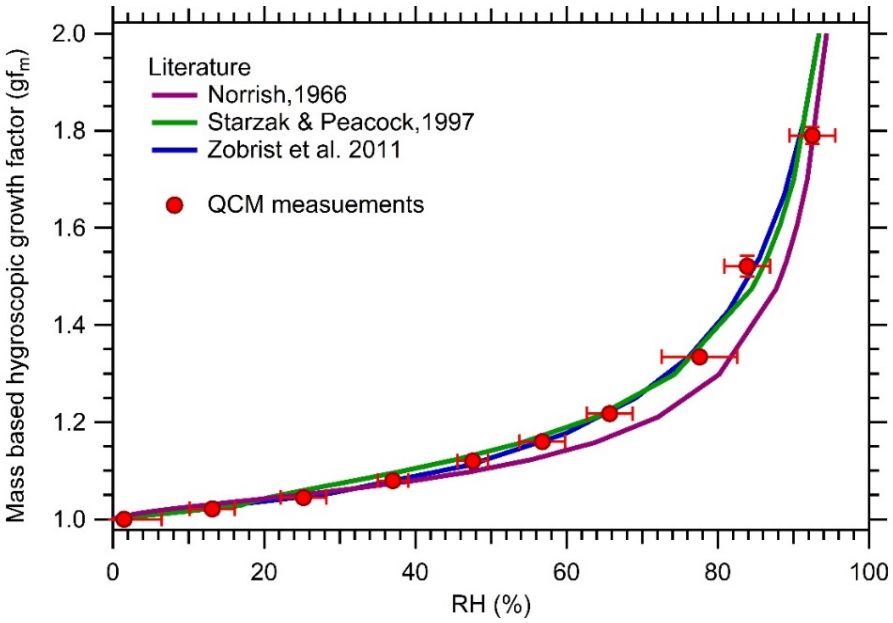

Figure S3. Mass-based hygroscopic growth factor gf_m of amorphous sucrose particles at different RH values in the subsaturated region obtained from the quartz crystal microbalance (QCM) measurements. The experimental values strictly follow the gf_m values retrieved using different models (Norrish, Starzak and Peacock, and Zobrist) from the literature.

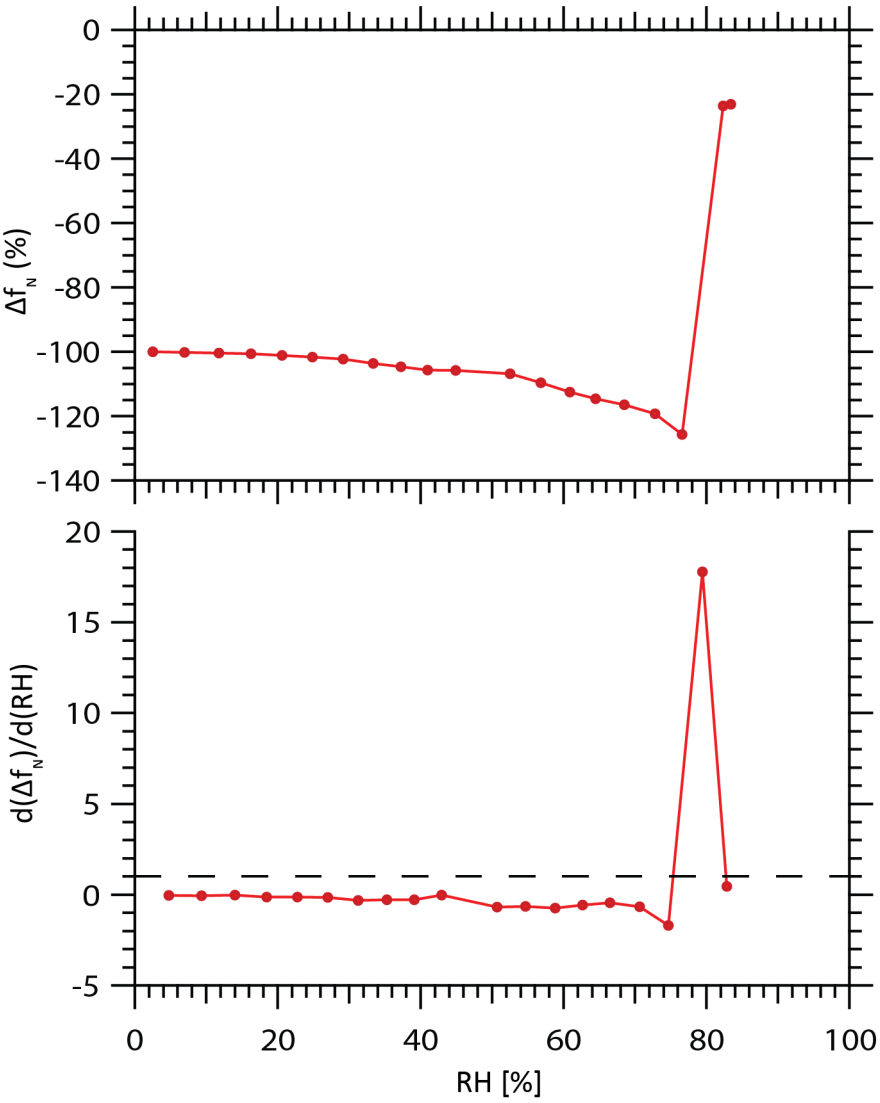

Figure S4. The deliquescence phase transition behavior of laboratory-generated $(NH_4)_2SO_4$ particles. Δf_N represents the change in the oscillation frequency of the quartz crystal microbalance (QCM) sensor resulting due to water uptake by the particles at different RH conditions normalized to that of the dry particles at RH <5%, expressed as percentage. The decrease in the value of Δf_N indicates the water uptake at different RH conditions in the sub-saturated region. The derivative of Δf_N with respect to RH, $d(\Delta f_N)/d(RH)$ is plotted against different RH conditions and the respective RH values for $d(\Delta f_N)/d(RH) \geq 1$, marked by the black dotted line, represent the deliquescence relative humidity (DRH) range (76-80%) for the $(NH_4)_2SO_4$ particles.

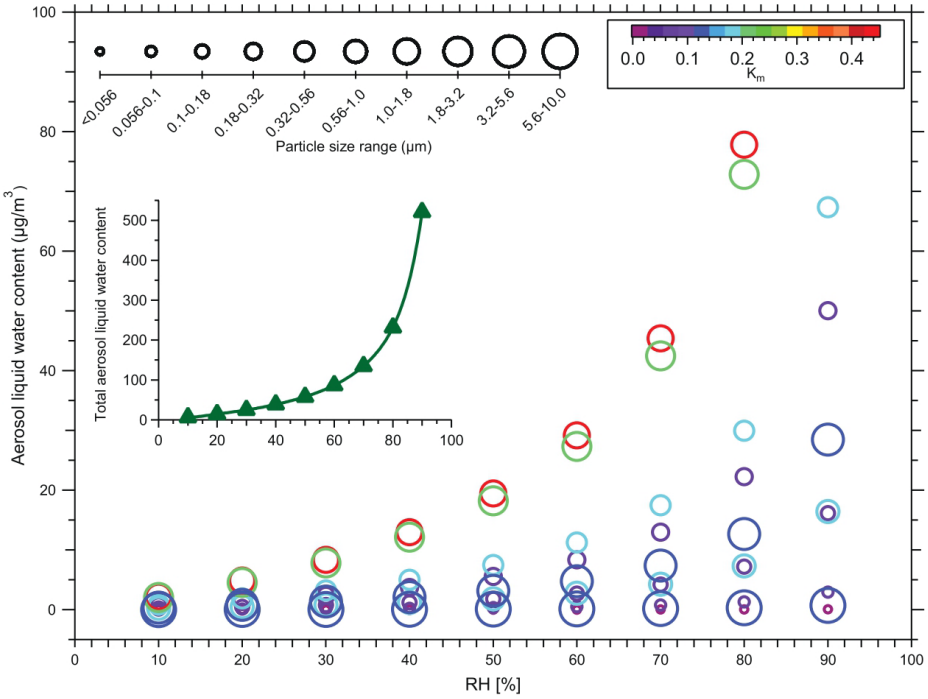

Figure S5. Aerosol Liquid Water Content (ALWC) in size-resolved ambient aerosol particles from Munnar across varied relative humidity (RH) conditions in the subsaturated regime. ALWC under different RH conditions is estimated by integrating size-resolved hygroscopic growth factor values with particle number size distribution (PNSD) measurements, assuming volume conservation during aerosol water uptake processes. The marker sizes correspond linearly to particle size, while marker colors signify the mean value of the mass-based hygroscopicity parameter (κ_m) for each size-range, indicated by the color palette. The total ALWC averaged over all particles below 10 µm in size is also shown in inset.

References:

Arenas, K. J. L., Schill, S. R., Malla, A., & Hudson, P. K. (2012). Deliquescence phase transition measurements by quartz crystal microbalance frequency shifts. *Journal of Physical Chemistry A*, *116*(29), 7658–7667. https://doi.org/10.1021/jp3016722

Bian, Y. X., Zhao, C. S., Ma, N., Chen, J., & Xu, W. Y. (2014). A study of aerosol liquid water content based on hygroscopicity measurements at high relative humidity in the North China Plain. *Atmospheric Chemistry and Physics*, *14*(12), 6417–6426. https://doi.org/10.5194/acp-14-6417-2014

Chao, H. J., Huang, W. C., Chen, C. L., Chou, C. C. K., & Hung, H. M. (2020). Water Adsorption vs Phase Transition of Aerosols Monitored by a Quartz Crystal Microbalance. *ACS Omega*, *5*(49), 31858–31866. https://doi.org/10.1021/acsomega.0c04698

Gupta, P., Banerjee, A., & Gupta, N. J. (2020). Spatio-temporal study on changing trend of land use and land cover pattern in Munnar area, Idukki district, Western Ghats, India. *Indian Journal of Geo-Marine Sciences*, *49*(6), 1055–1067.

Kale, M. P., Chavan, M., Pardeshi, S., Joshi, C., Verma, P. A., Roy, P. S., Srivastav, S. K., Srivastava, V. K., Jha, A. K., Chaudhari, S., Giri, Y., & Krishna Murthy, Y. V. N. (2016). Land-use and land-cover change in Western Ghats of India. *Environmental Monitoring and Assessment*, *188*(7). https://doi.org/10.1007/s10661-016-5369-1

Liu, P., Song, M., Zhao, T., Gunthe, S. S., Ham, S., He, Y., Qin, Y. M., Gong, Z., Amorim, J. C., Bertram, A. K., & Martin, S. T. (2018). Resolving the mechanisms of hygroscopic growth and cloud condensation nuclei activity for organic particulate matter. *Nature Communications*, *9*. https://doi.org/10.1038/s41467-018-06622-2

Marple, V., Olson, B., Romay, F., Hudak, G., Geerts, S. M., & Lundgren, D. (2014). Second generation micro-orifice uniform deposit impactor, 120 MOUDI-II: Design, Evaluation, and application to long-term ambient sampling. *Aerosol Science and Technology*, *48*(4), 427–433. https://doi.org/10.1080/02786826.2014.884274

Martin, S. T. (2000). Phase transitions of aqueous atmospheric particles. *Chemical Reviews*, *100*(9), 3403–3453. https://doi.org/10.1021/cr990034t

Mikhailov, E., Merkulov, V., Vlasenko, S., Rose, D., & Pöschl, U. (2013). Mass-based hygroscopicity parameter interaction model and measurement of atmospheric aerosol water uptake. *Atmospheric Chemistry and Physics*, *13*(2), 717–740. https://doi.org/10.5194/acp-13-717-2013

Norrish, R. (1966). Equation for the activity coefficients and equilibrium relative humidities. *JInternational Journal of Food Science & Technology*, *1*, 25–39.

Peng, C., Chen, L., & Tang, M. (2022). A database for deliquescence and efflorescence relative humidities of compounds with atmospheric relevance. *Fundamental Research*, *2*(4), 578–587. https://doi.org/10.1016/j.fmre.2021.11.021

Petters, M. D., & Kreidenweis, S. M. (2007). A single parameter representation of hygroscopic growth and cloud condensation nucleus activity. *Atmospheric Chemistry and Physics*, *7*(8), 1961–1971. https://doi.org/10.5194/acp-7-1961-2007

Rodahl, M., & Kasemo, B. (1995). On the measurement of thin liquid overlayers with the quartz-crystal microbalance. *International Conference on Solid-State Sensors and Actuators, and Eurosensors IX, Proceedings*, *2*, 743–746. https://doi.org/10.1109/sensor.1995.721939

Rose, D., Gunthe, S. S., Mikhailov, E., Frank, G. P., Dusek, U., Andreae, M. O., & Pöschl, U. (2008). Calibration and measurement uncertainties of a continuous-flow cloud condensation nuclei counter (DMT-CCNC): CCN activation of ammonium sulfate and sodium chloride aerosol particles in theory and experiment. *Atmospheric Chemistry and Physics*, *8*(5), 1153–1179. https://doi.org/10.5194/acp-8-1153-2008

Starzak, M., & Peacock, S. D. (1997). Water activity coefficient in aqueous solutions of sucrose -a comprehensive data analysis. *Zuckerindustrie*, *122*(5), 380–387.

Zobrist, B., Soonsin, V., Luo, B. P., Krieger, U. K., Marcolli, C., Peter, T., & Koop, T. (2011). Ultra-slow water diffusion in aqueous sucrose glasses. *Physical Chemistry Chemical Physics*, *13*(8), 3514–3526. https://doi.org/10.1039/c0cp01273d